Summer 2014

Gold-magnetite nanoparticle-biomolecule conjugates: synthesis, properties and toxicity studies

Akshay Pariti

Department:

GOLD-MAGNETITE NANOPARTICLE-BIOMOLECULE CONJUGATES: SYNTHESIS, PROPERTIES AND TOXICITY STUDIES

by

AKSHAY PARITI

A THESIS

Presented to the Faculty of the Graduate School of the

MISSOURI UNIVERSITY OF SCIENCE AND TECHNOLOGY

In Partial Fulfillment of the Requirements for the Degree

MASTER OF SCIENCE IN CHEMICAL ENGINEERING

2014

Approved by

Xinhua Liang, Advisor

Manashi Nath, Co-Advisor

Douglas Ludlow

PUBLICATION THESIS OPTION

This thesis consists of the following article that has been submitted for publication as follows:

Pages 15-40 have been submitted to MATERIALS RESEARCH EXPRESS.

ABSTRACT

This thesis study focuses on synthesizing and characterizing gold-magnetite optically active magnetic nanoparticle and its conjugation with biomolecules for biomedical applications, especially magnetic fluid hyperthermia treatment for cancerous tissue. Gold nanoparticles have already displayed their potential in the biomedical field. They exhibit excellent optical properties and possess strong surface chemistry which renders them suitable for various biomolecule attachments. Studies have showed gold nanoparticles to be a perfect biocompatible vector. However, clinical trials for gold mediated drug delivery and treatment studied in rat models identified some problems. Of these problems, the low retention time in bloodstream and inability to maneuver externally has been the consequential. To further enhance their potential applications and overcome the problems faced in using gold nanoparticles alone, many researchers have synthesized multifunctional magnetic materials with gold at one terminal. Magnetite, among the investigated magnetic materials is a promising and reliable candidate because of its high magnetic saturation moment and low toxicity. This thesis showcases a simple and facile one pot synthesis of gold-magnetite nanoparticles with an average particle size of 80 nm through hot injection method. The as-synthesized nanoparticles were characterized by XRD, TEM, Mössbauer spectroscopy, SQUID and MTS toxicity studies. The superparamagnetism of the as-synthesized nanoparticles has an interestingly high saturation magnetization moment and low toxicity than the literature values reported earlier. L-cysteine and (-)-EGCG (epigallacatechin-3-gallate) were attached to this multifunctional nanoparticles through the gold terminal and characterized to show the particles applicability through Raman, FTIR and UV-Vis spectroscopy.

ACKNOWLEDGMENTS

It is a pleasure presenting this thesis which could not have reached fruition with the support, patience and guidance of the following people. It is to them that I owe my deepest gratitude. First of all, I would like to thank my advisors Dr. Manashi Nath and Dr. Xinhua Liang for their insight and guidance throughout the process. Dr. Manashi Nath was very understanding and patient with me from the beginning. This research work would not have been complete without her intellectual insight and constructive criticism. I thank Dr. Xinhua Liang for his constant encouragement and invaluable discussions about my academics and research. I would also like to thank Dr. Douglas Ludlow for being on my committee along with my advisors, Dr. Kartik C. Ghosh for SQUID measurements, Dr. Amitava Choudhury for Mössbauer study and Dr. Nuran Ercal for the cell studies.

I am grateful to the entire faculty and staff of the Chemical Engineering and Chemistry departments of Missouri S&T for helping me grow as a better student over the past two years. Also, I am indebted to the faculty and staff of the Materials Research Centre for their instruments access on an as needed basis. I would also like to thank my fellow graduate students, especially Prachi Desai, Sukhada Mishra and Wipula Liyange for being there for me through hardships. Without their guidance and training at initial stages, it would have been very difficult. It is very difficult to mention the names of all the people who were linked directly or indirectly with this work and I extend my gratitude to all of them.

On a personal note, I would like to dedicate this thesis to my late father, P.V.R. Moorty and my wonderful mother, Revathi Peri, for her constant support, encouragement and unconditional love throughout my life for as far as I can remember.

TABLE OF CONTENTS

LIST OF ILLUSTRATIONS

SECTION

LIST OF TABLES

1. INTRODUCTION

Nanobiotechnology, the combination of nanotechnology and molecular biology is a tremendously powerful technology. It holds a huge promise for the design and development of many types of novel products with potential applications in the fields of biology and medicine, including early disease detection through advanced noninvasive medical imaging, treatment through high site-specific drug delivery and protein purifications. Many metal nanoparticles have been synthesized using various synthetic methods for this purpose. Among all the candidates investigated, gold nanoparticles have proven to be extremely useful and reliable candidate. They serve as highly biocompatible vectors capable of selective and nuclear targeting for site-specific diagnosis and treatment with extremely low toxicity. Hence, gold nanoparticles were synthesized in different morphologies including nanoshells, nanorods, tripods, nanocages and nanotubes for various applications. Despite their numerous advantages, researchers have found some disadvantages such as the lack of ability to manipulate them externally and low retention time in the bloodstream.

To overcome these disadvantages and for the potential benefits of multimodal functionality in biomedical applications, researchers have attached gold with other magnetic materials. These attached nanomaterials are more precisely described as multifunctional magnetic nanomaterials, since they exhibit two or more distinctively different functionalities within a single nanostructure. One of the successful and promising multifunctional magnetic nanomaterials is the gold-magnetite (Au-Fe_3O_4) nanoparticles because magnetite offers high magnetization saturation moment and susceptibility with low toxic nature. Magnetite nanoparticles by themselves have also demonstrated their potential for biomedical applications in magnetic resonance imaging (MRI) and hyperthermia (local heat treatment for destruction of cancer cells). This research work outlines the synthesis, characterization of gold-magnetite (Au-Fe_3O_4) nanoparticles and their conjugation with biomolecules such as L-cysteine and (-)-EGCG (epigallocatechin-3-gallate).

1.1. GOLD NANOPARTICLES: PROPERTIES AND APPLICATIONS

Gold is one of the subjects for most ancient themes of investigation in science.[1] Its renaissance now leads to an exponentially increasing number of publications for its applications in electronic, medical and biological fields, especially in context with the emerging nanoscience and nanotechnology. Gold nanoparticles are mostly isolated as stable colloidal solution of clusters of gold atoms in the size range of 1-100 nm. They are amongst the most stable metal nanoparticles. In this dimensions, gold nanoparticles exhibit some special optical properties when compared to bulk gold.[2,3] For example, the color changes from yellow to ruby red when bulk gold is converted to gold nanoparticles. This change in color can be explained using the "surface plasmon resonance" theory (figure 1.1).

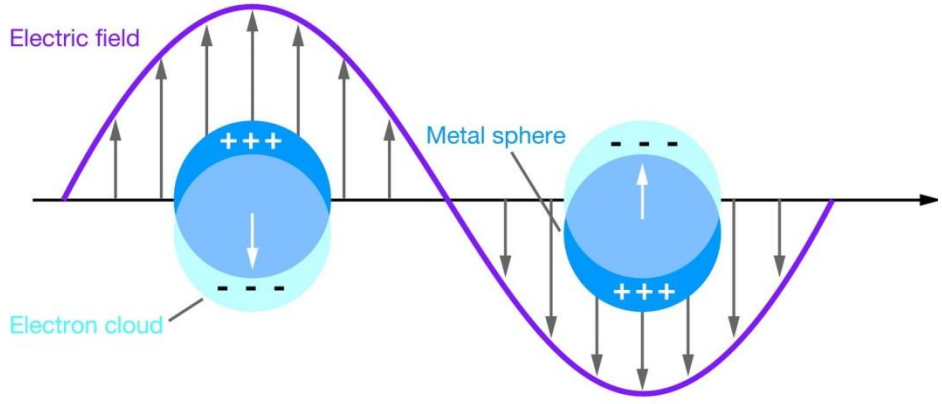

Figure 1.1. Schematic representation of a localized surface plasmon. Reprinted with permission from reference 4. Copyright 2007 by Annual Reviews.

Surface plasmon resonance[5] theory states that when a cluster of gold atoms are hit by an electromagnetic field, the surface electrons of the gold atoms (occupying the 6s levels of the gold-atom clusters) present in the conduction band of gold nanoparticles oscillate back and forth, creating a plasmon band with an absorption peak in the visible region at 520-550 nm. Gustav Mie proposed an explanation for the phenomenon[6] in 1908 which rationalizes the nature of surface plasmon resonance. According to Mie theory, the total cross section composed of the surface plasmon absorption and scattering is the summation over all the electric and magnetic oscillations. These surface plasmons were described quantitatively by solving Maxwell's equations for spherical particles with appropriate boundary conditions. Thus, surface plasmon resonance band is absent for

gold nanoparticles with size less than 2 nm and greater than 500 nm. The surface plasmon resonance band maximum and bandwidth are also influenced by the particle shape, medium dielectric constant and refractive index of the solvent in which gold nanoparticles are suspended, density of electrons and effective electron mass. For small spherical particles, the collective oscillation of electrons is called dipole plasmon resonance of the particle. As the geometry of the nanoparticles changes, these boundary conditions are no longer valid. Modern day approaches such as discrete dipole approximation[7] can applied to calculate the surface plasmon absorption for arbitrary geometries. These approaches account for the longitudinal plasmon resonance or quadrupole plasmon resonance which is in accordance with experimental values. The increase in intensity and wavelength maximum as the aspect ratio (length divided by breadth) increases. Figure 1.2 represents the change in absorption spectra as the shape and size of gold nanoparticles varies.

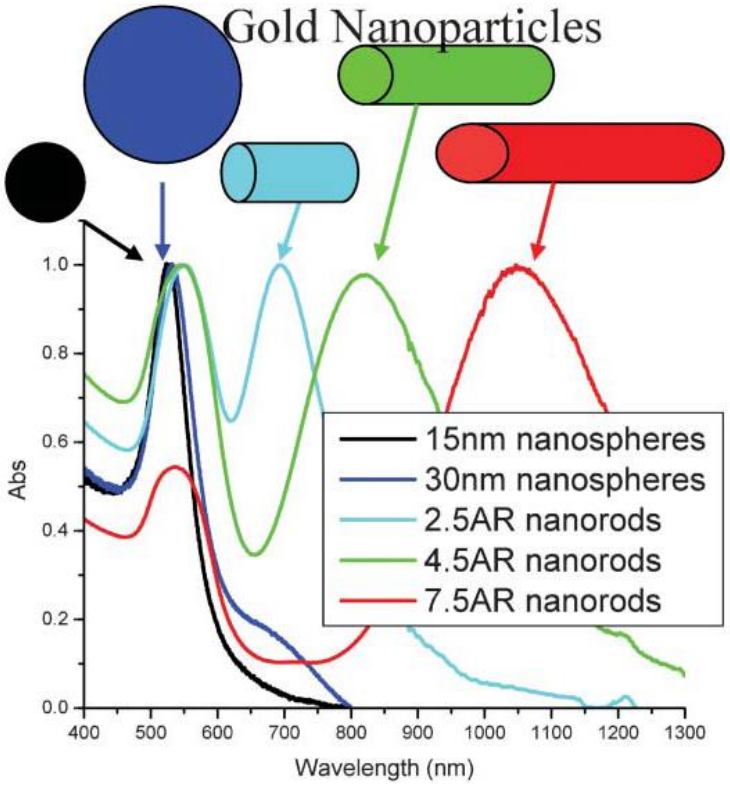

Figure 1.2. Gold nanoparticles-absorption spectra of various sizes and shapes. Reproduced from reference 8 with permission of The Royal Society of Chemistry. Copyright 2005 by Royal Society of Chemistry.

Several research groups have fabricated gold nanoparticles with monodispersity and controlled size by reduction of gold salts in presence of appropriate stabilizers that prevent particle agglomeration. Electro deposition and physical methods like sonochemistry, radiolysis have also been employed for their synthesis. Some of the most common synthetic methods are listed in table 1.1.

Table 1.1. Common synthetic methods and capping agents for gold nanoparticles

Core size (nm)	Synthetic methods	Capping agents
1-2	Reduction of $AuCl(PPh_3)$ with diborane or sodium borohydride.[9]	Phosphine (PR_3; R= alkyl groups)
1.5-5	Biphasic reduction of $HAuCl_4$ by sodium borohydride.[10,11]	Alkanethiol
10-150	Reduction of $HAuCl_4$ with sodium citrate.[12]	Citrate

The affinity of gold towards the sulfur head of the thiols and amines make them very responsive towards biofunctionalization with appropriate biomolecules, leading to significant medical and biological applications.[13,14,15] Figure 1.3 illustrates some of the biomedical applications of gold nanoparticles and few applications are discussed in detail later.

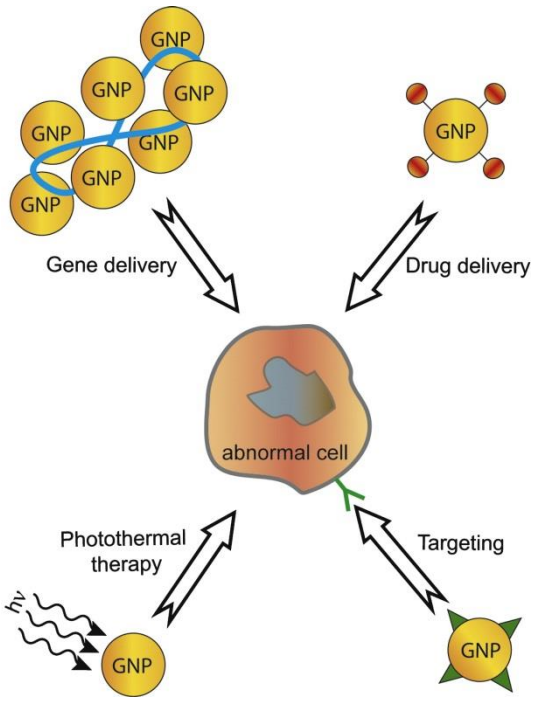

Figure 1.3. Biomedical applications of gold nanoparticles. Reprinted from reference 14 with permission from Elsevier. Copyright 2008 by Elsevier.

1.1.1. Bio-Sensing. Gold nanoparticles based bio-sensors[12] functions by detecting the change insensitivity of plasmon resonance frequency as it is a very reliable intrinsic feature. The binding of biomolecules to the surface of gold nanoparticles can change the plasmon resonance frequency directly. This change in the plasmon resonance frequency is called plasmon coupling and can be used for colorimetric detection of analytes. This method was first pioneered by Mirkin et al. who developed an assay for the detection of DNA.[16,17] In this assay, the gold nanoparticles were conjugated with oligonucleotides containing sticky ends that are complementary to the target sequence which is to be detected. The initial color of the conjugated gold nanoparticles appeared red but after hybridization with the target sequence, the colloidal solution appeared violet-purple. Several other DNA assays have been developed based on this concept for quantitative analysis and the same concept can be applied for other analytes apart from DNA. Also, from the change in color one can predict the change in size of the gold nanoparticles.

1.1.2. Hyperthermia. Hyperthermia is a local heat generation technique to kill cancerous cells by stimulating the nanoparticles with an external stimulus, in this case light. When gold nanoparticles absorb light, the free electrons on the surface are excited. This excitation causes collective oscillation of the free electrons. Interaction of these free electrons with the crystal lattice causes the electrons to relax by transferring the thermal energy to the lattice. Subsequently, the heat is dissipated to the surrounding environment.[18,19] The ideal average human body temperature is 37°C. Body temperatures between 37-42°C can lead to fever and above 42°C can be lethal.[20] Hyperthermia is based on this fact and is carried out in two steps. First, gold nanoparticles conjugated with specific receptors for cancerous cells are enriched in the cancerous tissue (i.e. cell internalization). Second, the particles are excited by an external stimulus to generate heat and dissipate to the surroundings for selective killing.

1.1.3. Contrast Based Imaging. Imaging studies are based on the comparisons of contrast produced by variations in the electron densities from different tissues. Since, gold nanoparticles have high electron density; they can effectively be used as contrast enhancing imaging agents. Again, the gold nanoparticles are conjugated with the appropriate biomolecules to target the specific tissue or organ and administered in to the body. When the particles are administered and enter the bloodstream, they bind to the specific organ or tissue through receptor-ligand interactions. The particles bound to the tissue or organ provides high contrast difference for better imaging. Gold nanoparticles can be imaged with high signal to noise ratio by X-ray computer tomography with short exposure time, which helps in reduced damage to the nearby tissues through long exposed radiation sessions, if needed.[21,22]

1.1.4. Targeted Drug Delivery. Cells have the ability to ingest nanoparticles naturally, so nanoparticle incorporation can be specific (via receptor-ligand interaction) or non-specific.[23] After the ingestion, cells store the ingested nanoparticles in endosomal/lysosomal vesicular structures in them.[24] For successful release of the particles to the cytosol, the nanoparticle surface can be coated with disruptive polymer or peptide which allows their direct entry in to the cytosol.[25,26] Gold nanoparticles can be modified by conjugation with various drug molecules and coating for release into cytosol depending on the specific uptake of the targeted cells while retaining their

biocompatibility. Generally, they are used in gene therapy[27] and anti-cancer drug delivery to cancerous cells.[28]

1.2. MAGNETITE NANOPARTICLES: PROPERTIES AND APPLICATIONS

Iron oxide is a generic name given for iron oxides, hydroxides, oxyhyrdoxides and other related compounds. All together there are 16 different types of compounds known. Among them, magnetite, Fe_3O_4 is the most magnetic and naturally abundant mineral. Loadstone, a naturally magnetized form of magnetite was historically used by navigators to locate the geographic north. They were also used as pigments in paints and paleomagnetism (tectonic plate studies). Recently, magnetite nanoparticles have become important due to their widespread applications such as ferrofluids,[29] digital media recording,[30] MRI contrast agents,[31] targeted drug delivery,[32] magnetic hyperthermia,[33] sorbent for wastewater treatment[34] etc.

Magnetite has an inverse spinel structure with $Fd\bar{3}m$ space group. The unit cell is made up of eight formula units. It has oxygen in cubic close packed lattice with Fe^{3+} occupying the tetrahedral and octahedral sites, where it co-exists with Fe^{2+}in the octahedral sites. Thus the formula for magnetite can be precisely written as $tetFe^{3+}[OctFe^{3+}Fe^{2+}]O_4$. The tetrahedral site is often referred as A site and octahedral site as B site. There are 16 Fe^{3+} ions with equal distribution on A and B sites, 8 Fe^{2+} ions on the B site and 32 O atoms.

Generally, magnetic materials can be classified as paramagnetic, ferromagnetic, ferrimagnetic or anitferromagnetic based on the orientation of the magnetic dipoles within the material in presence of an external magnetic field (figure 1.4). Magnetic behavior of a material is strongly dependent on size of the material, temperature and the applied magnetic field. Bulk magnetite is a ferrimagnetic material, however magnetite nanoparticles exhibit superparamagnetism.[35,36] It is the nano-size effect of ferro or ferrimagnetism. Below a critical size, a ferro or ferrimagnetic material is reduced to a state which consists of single magnetic domain and with no internal domain boundaries. It is in a state of unified magnetization within the particle at any applied field. The direction of collective magnetization of an ensemble can rotate thermally and behave as a superparamagnet with a very large moment (figure 1.5).

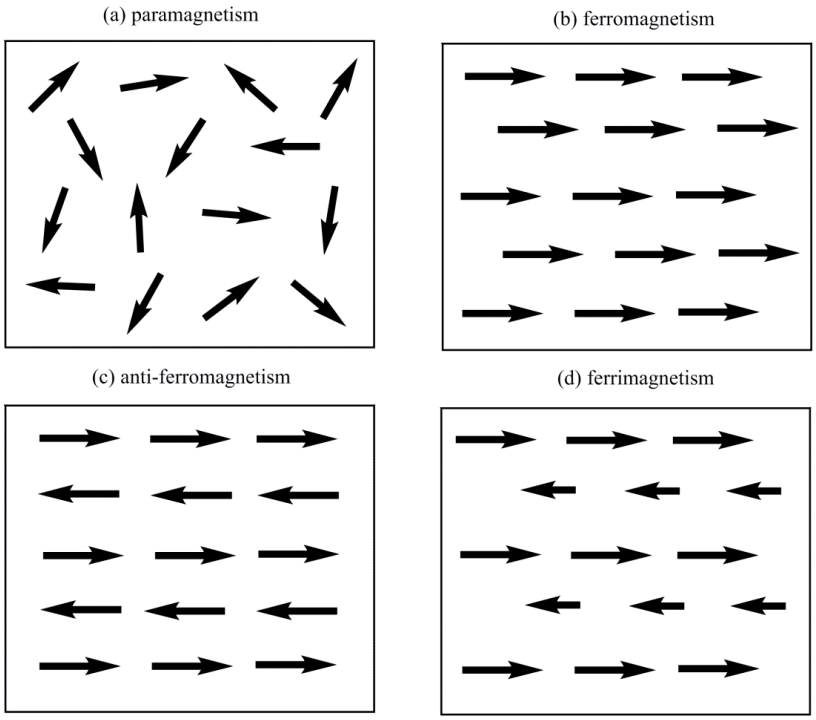

Figure 1.4. Magnetic ordering in (a) paramagnetic, (b) ferromagnetic, (c) anti-ferromagnetic and (d) ferrimagnetic materials.

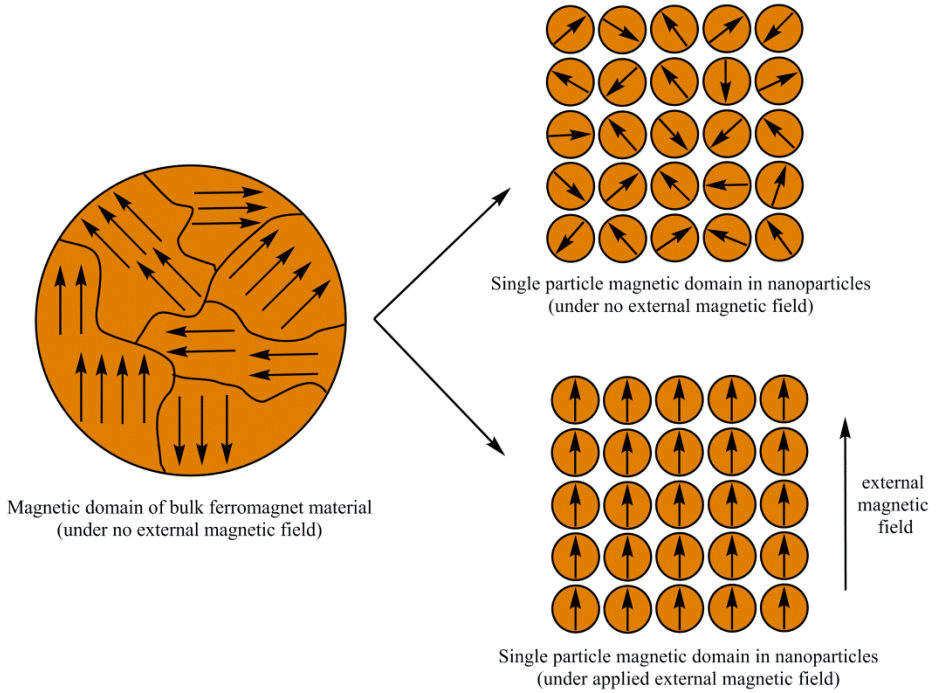

Figure 1.5. Schematic representation of magnetic ordering in bulk ferromagnet material and single particle domain (in absence and presence of external magnetic field).

Frenkel and Dorfman[37] were the first to predict this behavior. Later, Kittel[38] and others estimated the critical dimension for a spherical particle of common ferromagnetic materials. In 1949, Neel pointed out that if the single domain particles were small enough, thermal fluctuations could cause its direction of magnetization to undergo a sort of Brownian motion and also derived an equation for the particles to arrive at thermal equilibrium in a given time. In 1959, Bean and Livingston[39] explained superparamagnetism using a model system of spherical particles with uniaxial anisotropy that were first fully magnetized along the easy axis of symmetry. By considering spherical particles, the magnetic anisotropy can be approximated to be proportional to the particle volume, *V*. To approach zero remanence corresponding to thermal equilibrium, a sufficient number of particles must be reversed by thermal activation. The energy barrier that separates easy magnetization axes is the magnetic anisotropy energy, K_vV, where K_v is the volume anisotropy constant (figure 1.6). For nanoparticles, the particle size is small and the magnetic anisotropy energy is comparable with thermal energy (equation 1.1). Thus, the magnetic moment of the particle may fluctuate behaving as a superparamagnet but with a total moment exceeding that of the bulk by approximately 1000 times.

$$K_vV \leq 25k_BT \qquad \ldots(1.1)$$

Now applying the Boltzmann distribution for the total magnetization of the particles ensemble when subjected to external applied field and thermal equilibrium can be given by *Langevin* equation (equation 1.2).

$$M = Mo\left[\coth\left(\frac{\mu H}{k_BT}\right) - \frac{1}{\left(\frac{\mu H}{k_BT}\right)}\right] \qquad \ldots(1.2)$$

Where M = magnetization, M_0 = saturation magnetization, H = applied magnetic field, μ = magnetic moment, T = temperature and k_B = Boltzmann constant.

Besides, the dependence of magnetization on particle size, shape and composition it greatly depends on temperature also. The critical temperature above which ferro or ferrimagnetic particle will behave as superparamagnetic, a state where spontaneous fluctuations of the particle moment are allowed causing loss of magnetic ordering is called as blocking temperature (T_B)[39,40] and can be predicted by equation 1.3 i.e. thermal energy is equal to the magnetic anisotropy energy.

$$T_B = \frac{K_vV}{25k_B} \qquad \ldots(1.3)$$

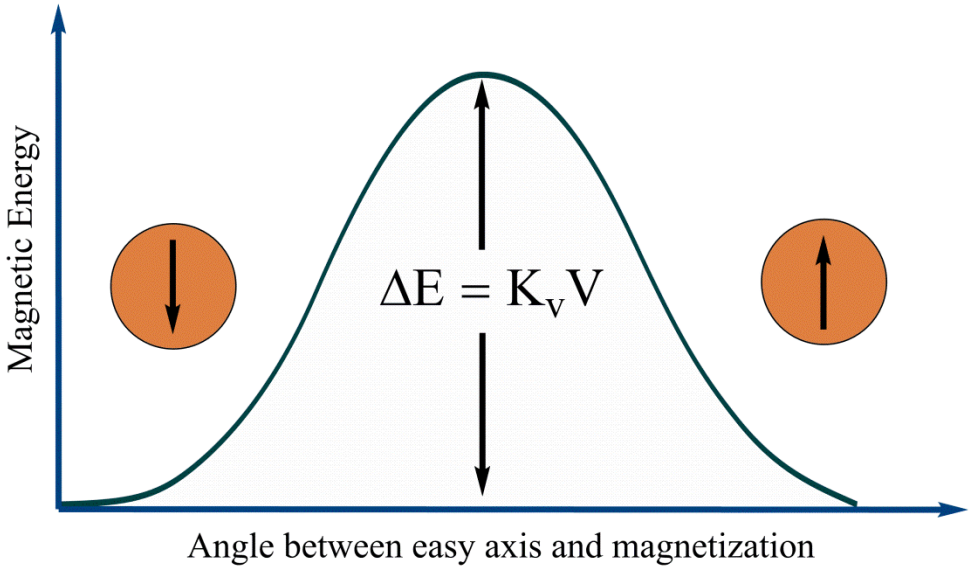

Figure 1.6. Schematic representation of the magnetic energy versus angle between easy axis of magnetization and applied magnetic field.

In 1939, Verwey[41] observed a phase transition (cubic to triclinic) in magnetite below 120 K due to first order transition. The resistivity of magnetite increased by a factor of the order 100 due to this transformation. This was later explained by charge ordering of divalent and trivalent ions on the octahedral sites in alternation layers.[42] This temperature at which phase transformation occurs is called Verwey temperature (T_V). When the particle size reduces from bulk to nanoparticle regime, the Verwey temperature decreases or disappears.

Superparamagnetic particles by virtue of their unique magnetic properties show usefulness in avariety of diverse applications. Superparamagnetic magnetite nanoparticles are being used for the following applications due to high magnetization saturation moment and low toxicity.

1.2.1. Ferrofluid. Ferrofluids[29,43] are colloidal suspensions of permanently magnetized nanoparticles in a carrier fluid, usually organic solvent or water with no long range ordering. Brownian motion keeps them from settling and the influence of gravity and the coating around these particles provide short range steric repulsions which prevent particle agglomeration under non uniform magnetic field. Ferrofluid was first invented by NASA's Steve Papella[44] as a low density and low viscosity magnetic propellant usable under zero gravity conditions. These ferrofluids also have potential applications in

micro/nanoelectromechanical systems (MEMS/NEMS), analytical and medical devices, sealing, heat transfer, bearing etc.

1.2.2. Wastewater Remediation. Industrial wastewater contains hexavalent chromium compounds that usually exist as chromate (CrO_4^{2-}) and dichromate ($Cr_2O_7^{2-}$). They are highly toxic agents that act as carcinogens and mutagens. So their treatment is very important and generally carried out by applying a reducing agent such as ferrous sulfate. This method consumes large quantities of reagents, utilizes large volume sludge treatment reactors and is a high cost operation. Whereas using magnetite nanoparticles overcomes these problems with additional advantages. The advantages include (i) utilization of minimal quantity of nanoparticles, (ii) higher adsorption capacity of nanoparticles due to larger surface area, (iii) regeneration of the nanoparticles by desorption technique is easy and faster, (iv) ease of separation from treated water by using external magnetic field.[45,46,47]

1.2.3. Biological Applications. Similar to gold nanoparticles, the surface of the magnetite nanoparticles can be functionalized and can be used for various biological applications such as magnetic fluid hyperthermia, MRI, targeted drug delivery etc. Researchers have used the magnetite nanoparticles conjugated with TAT protein derived peptide sequence to tag cells magnetically for effective imaging. Another promising application of these magnetite nanoparticles is in drug delivery. Widder *et al.* demonstrated the usefulness of magnetic albumin microspheres in animal tumor models.[48] These modified microspheres achieved significantly greater responses than adriamycin alone. Gallo *et al.* have later demonstrated the same in normal rats.[49] In their work, they report that the retention time of these microspheres was up to 72 hours. Other researcher groups have also proved magnetite nanoparticles effective use in DNA analysis, cell separations, cell specific targeting and hyperthermia.[33,50,51]

Significant efforts have been devoted in the synthesis of magnetite nanoparticles with different characteristics for various applications. Some of the common methods include hydrothermal treatment, thermal decomposition, co-precipitation, sonochemical and solvothermal.[50,51] Among them, thermal decomposition and co-precipitation are the most common techniques adopted by researchers. The co-precipitation process involves the precipitation of iron precursors Fe^{2+} and Fe^{3+} in the ration of 1:2 by using an alkali,

usually sodium hydroxide or ammonium hydroxide, which leads to the formation of a black precipitate of magnetite nanoparticles. On the other hand, thermal decomposition process involves decomposition of an organic precursor for the formation of magnetite nanoparticles in presence of capping agents, usually eqimolar mixture of oleic acid and oleylamine. Some common synthetic techniques are listed below in table 1.2.

Table 1.2. Common synthetic methods and reaction factors for magnetite nanoparticles

Synthetic methods	Reaction Factors
Co-precipitation of divalent and trivalent iron salts, usually chloride or sulfate salts[52,53,54]	8≤ pH ≤12, ratio of divalent iron to trivalent iron = 2:1
Hydrothermal synthesis[55]	Solvent, temperature and time
Thermal decomposition[56,57]	Surfactant, stabilizer, temperature

1.3. MULTIFUNCTIONAL MAGNETIC MATERIALS

From the earlier sections, it can be stated that gold and magnetite nanoparticles have potential benefits in electronic, mechanical, biological and medical applications. But they have their own disadvantages too. Gold nanoparticles have short circulation time in the bloodstream and only a small fraction of the particles have a chance to bind with the organ or tissue when used as MRI contrast agents. They are readily cleared in the body by the liver and kidneys. The other problem faced by using gold nanoparticles for hyperthermia is that the local particle enrichment. Tissues absorb light in the visible region and infrared light can only penetrate through thin tissues. Therefore, gold nanoparticles can be used for tissues close to the skin and not deep inside. Magnetite nanoparticles on the other hand also have some disadvantages despite their potential applications. For colloidal suspensions of magnetite nanoparticles, a polymeric or organic

coating is indispensable. Also, unlike gold nanoparticles, magnetite nanoparticles cannot bind with a wide range of biomolecules.[13,50]

Hence, to overcome these problems researchers have devoted significant amount of time and hard work to attach gold with magnetite nanoparticles using different synthetic techniques. Several groups have reported the formation of gold-magnetite nanoparticles in different morphologies such as core-shell, core-hollow shell, dumbbell shape, nanoflower etc.[58,59,60] S. Sun *et al.* have proposed a mechanism for the formation of these multifunctional nanomaterials.[58] They state that if a polar solvent is used in the synthesis process, the electron deficiency on the gold is replenished by the solvent itself which allows multiple nucleation sites to be formed. And as the process continues, the nucleation lobes grow, connect and eventually form a shell on the gold surface. If the synthesis process involves the utilization of non-polar solvent, once a single nucleated site depletes the electrons from gold, the electron deficiency cannot be replenished in the reaction i.e. solvent preventing the formation of new nucleation site on the gold surface. This process eventually results in formation of dumbbell shaped nanoparticles.

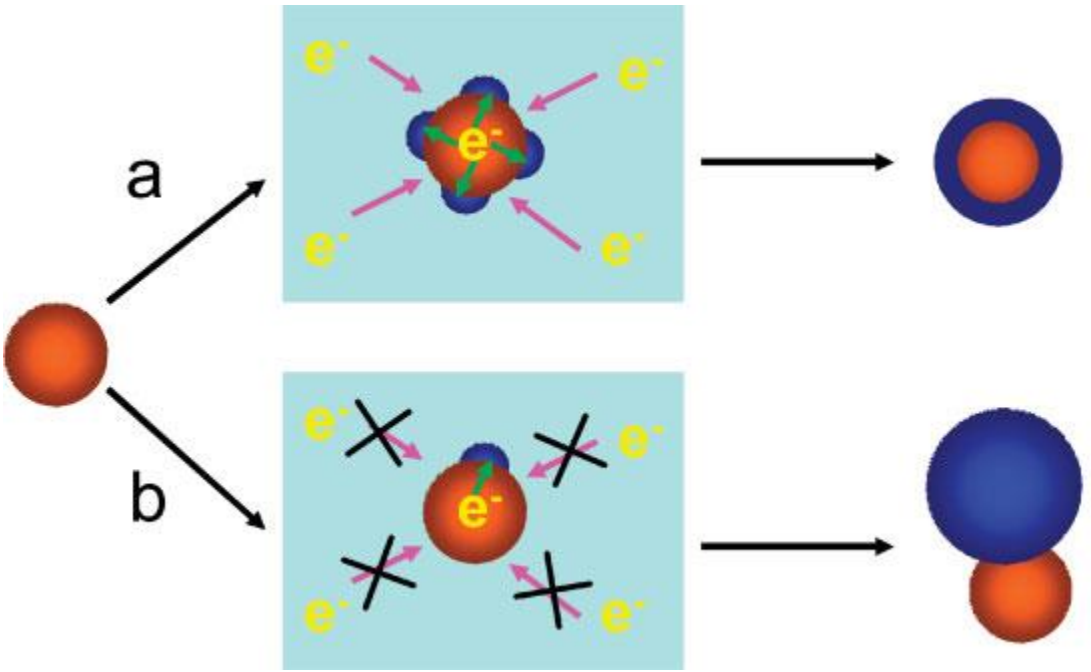

Figure 1.7. Schematic representation showing the mechanism of formation of (a) core shell nanoparticle (polar solvent) and (b) dumbbell shaped nanoparticles (non-polar solvent). Reused from reference 58 with permission from Wiley. Copyright 2008 by Wiley-VCH GmbH & Co. KGaA, Weinheim.

Multicomponent nanomaterials integrate several functionalities in a single particle ensemble. Hence, the plasmonic, magnetic and magneto-optical properties change when compared to the individual components alone. In the earlier section, it was stated that gold nanoparticles exhibit strong surface plasmon resonance absorption. These multicomponent nanomaterials also exhibit surface plasmon resonance absorption but it is significantly red shifted. The reason for this behavior can be given using Mie theory. Surface plasmon resonance depends on the refractive index, dielectric constant etc., and the attachment of magnetite to the gold alters these parameters causing the red shift in the absorption peak. Second, the magnetic properties of multicomponent nanomaterial also changes. The observed changes include decreased magnetization saturation, increased coercivity and decreased remanence ratio. This change in behavior can be explained by a new surface anisotropy induced by the attachment: Fe atoms at the interface have reduced number of nearest neighbors, which in turn decreases the interatomic exchange coupling. The new uniaxial anisotropy dominates the original cubic anisotropy i.e. the non-magnetic gold acts as a template blocking the spins at the interface.

1.4. RESEARCH PROBLEM

In context with the previous section topics it can be said that multifunctional magnetic nanomaterials are very important in biological and medical applications. The research problem for this thesis is the synthesis of multifunctional gold-magnetite nanoparticle-biomolecule conjugates with higher magnetization saturation moment and lower toxicity compared to earlier reported values, using novel synthesis routes. These bifunctional gold-magnetite nanoparticles were synthesized using one pot hot injection method. Further, the thesis also focuses on the validation of these nanoparticles and their conjugation with biomolecules like L-cysteine and (-)-EGCG using various microscopic and spectroscopic techniques such as SEM, TEM, Mössbauer and SQUID magnetization studies, Raman and FTIR, etc. The upcoming chapters deal with the experimental procedures followed and their results.

PAPER

I. SUPERPARAMAGNETIC Au-Fe_3O_4 NANOPARTICLES: ONE-POT SYNTHESIS, BIOFUNCTIONALIZATION AND TOXICITY EVALUATION

A Pariti[1], P Desai[2], S K Y Maddirala[2], X Liang[1], N Ercal[2], K V Katti[3] and M Nath[2]*

[1]Department of Chemical Engineering, Missouri University of Science and Technology, Rolla, MO 65409, U.S.A.

[2]Department of Chemistry, Missouri University of Science and Technology, Rolla, MO 65409, U.S.A.

[3]Departments of Radiology and Physics, University of Missouri, Columbia, MO 65212, U.S.A.

*Email: nathm@mst.edu

ABSTRACT

Superparamagnetic Au-Fe_3O_4 bifunctional nanoparticles have been synthesized using a single step hot-injection precipitation method. The synthesis involved using $Fe(CO)_5$ as iron precursor and $HAuCl_4$ as gold precursor in presence of oleylamine and oleic acid. Oleylamine helps in reducing Au^{3+} to Au^0 seeds which simultaneously oxidizes Fe(0) to form Au-Fe_3O_4 bifunctional nanoparticles. Triton® X-100 was employed as a highly viscous solvent to prevent agglomeration of Fe_3O_4 nanoparticles. Detailed characterization of these nanoparticles was performed by using X-ray powder diffraction, transmission electron microscopy, scanning tunneling electron microscopy, UV-visible spectroscopy, Mössbauer and magnetometry studies. To evaluate these nanoparticles applicability in biomedical applications, L-cysteine was attached to the Au-Fe_3O_4 nanoparticles and cytotoxicity of Au-Fe_3O_4 nanoparticles was tested using CHO cells by employing MTS assay. L-cysteine modified Au-Fe_3O_4 nanoparticles were qualitatively

characterized using Fourier transform infrared spectroscopy and Raman spectroscopy; and quantitatively using acid ninhydrin assay. Investigations reveal that that this approach yields Au-Fe_3O_4 bifunctional nanoparticles with an average particle size of 80 nm. Mössbauer studies indicated the presence of Fe in Fe^{3+} in A and B sites (tetrahedral and octahedral, respectively) and Fe^{2+} in B sites (octahedral). Magnetic measurements also indicated that these nanoparticles were superparamagnetic in nature due to Fe_3O_4 region. The saturation magnetization for the bifunctional nanoparticles was observed to be ~74 emu/g which is significantly higher than the previously reported Fe_3O_4 nanoparticles. Mössbauer studies indicated that there was no significant Fe(0) impurity that could be responsible for the superparamagnetic nature of these nanoparticles. None of the investigations showed any presence of other impurities such as Fe_2O_3 and FeOOH. These cysteine functionalized Au-Fe_3O_4 bifunctional nanoparticles showed no significant cytotoxicity to the CHO cells up to 48 h even at concentrations of 1 mg/ml making them suitable for biomedical applications such as local heat generators (hyperthermia) for cancer treatment and drug delivery vehicles.

1. INTRODUCTION

Multifunctional nanomaterials have recently attracted the attention of the materials science community owing to their vast applicability in a diverse range of applications [1-6]. One of the most promising applications for these multifunctional nanomaterials is related to the biomedical field where they have been used as photothermal killing of cancerous cells [7], magnetic resonance and fluorescence imaging [8-11], cell targeting and sorting [12], and drug delivery [13-15]. In these multifunctional nanostructures which are made by fusion of two entirely different materials with diverse properties into one single nanostructure, Au has been the preferred choice as one of the components. Traditionally, Au nanoparticles have demonstrated their importance in biological and medicinal applications, including immuno-sensing [16], phagokinetic studies [17], as carrier vehicles for delivery of nucleic acids via covalent and non-covalent conjugation [18], labelling and cell visualization by photothermal or photo acoustic methods [19], separation and purification of biomolecules, hyperthermia agents (local heat generation for tumor destruction), contrast enhancer, tissue engineering and highly selective bio-sensors[16-18]. The reason for their extensive applications in biology and medicine is not

only because of their robust interaction with biomolecules containing thiol and disulfide functional groups but also due to their unique optical properties. However, despite the numerous advantages, the ability to manipulate Au non-invasively is rather limited.

Recently, many researchers have tried to find a solution to this problem by using multifunctional nanomaterials where Au is combined with other suitable magnetic materials thereby producing an optically active magnetic nanostructure. Among these, magnetite (Fe_3O_4) is the most appropriate candidate to be coupled with Au, due to its low toxicity, high saturation magnetization and high susceptibility. Magnetite nanoparticles have also been used as drug delivery vehicle (therapeutics) [20], to generate local heat in alternating magnetic field leading to necrosis of cancer cells (hyperthermia) [21], MRI contrast enhancer and magnetic separator when labelled with appropriate biomolecules [22-26]. The functionality of the magnetic nanoparticles depends predominantly on their unique magnetic properties in the nanoscale including superparamagnetism. As the size of a ferromagnetic particle is reduced from the bulk state to below several tens of nanometers (i.e. critical size), the particle behaves as a monodomain magnetic particle. This behavior is termed as superparamagnetism and the material is called superparamagnetic [27]. The minimum temperature above which spontaneous flipping of the particle moment under an applied field occurs is called as the blocking temperature, T_B. Above T_B the particles behave as superparamagnets with randomly oriented particle moments, while below T_B they may exist in blocked (i.e. ordered) state.

As a bifunctional nanoparticle, gold-iron oxide nanoparticle can inherit excellent surface chemistry characteristics, unique optical properties (attributed to Au) and superparamagnetic characteristics attributed to Fe-oxides. Drugs attached to these bifunctional nanoparticles can have more advantages over ordinary drugs. First, they offer size controllability, ranging from few to hundreds of nanometers with different and unique size-dependent properties. Second, they can be easily controlled and manipulated from outside with the help of external magnetic field being operated from a distance. Third, they can provide enhanced contrast in medical imaging that can be used to diagnose the situation efficiently. Fourth, with their highly selective binding properties, drug molecules can also be attached to the surface of these nanoparticles. Fifth, they also exhibit high rate of absorption in the human body due to their high surface area to volume

ratio. These characteristics would further enhance and broaden the application of these nanoparticles for *theranostic* applications.

Given such importance of the gold-iron oxide nanoparticles in *theranostic* applications, there have been considerable efforts directed towards synthesis of these bifunctional nanoparticles. Reported synthesis protocols for Au-Fe_3O_4 include decomposition of iron precursors (e.g. iron acetylacetonate) on gold nanoparticle seeds, reduction of Au^{3+} on iron oxide nanoparticles with porous silica shell, by chemical bond linkage using intermediary molecules to form core-shell, core-hollow shell, and dumbbell-like nanostructures [28-34]. However, most of these methods were multi-step processes, which might be detrimental for large scale synthesis of these potentially transformative nanoparticles. Hence, there is still a need for producing these gold-iron oxide nanoparticles through simpler reactions involving less number of steps and more biocompatible precursors.

In this article we report a facile one-pot synthesis of bifunctional Au-Fe_3O_4 superparamagnetic nanoparticles and their biofunctionalization with simple amino acid like cysteine. These bifunctional nanoparticles were synthesized in a single step from reaction between $HAuCl_4$ and $Fe(CO)_5$ in presence of oleic acid and oleylamine. Magnetic and optical properties of these nanoparticles were studied in details. Cell viability and toxicity studies were also carried out on these nanoparticles which revealed that these were not toxic to CHO cells even at moderately high exposure. The superparamagnetic nature with high saturation magnetization and very low toxicity makes these Au-Fe_3O_4 nanoparticles very suitable for *theranostic* applications.

2. EXPERIMENTAL SECTION

2.1. Materials. Iron pentacarbonyl ($Fe(CO)_5$), oleylamine, ninhydrin, Dulbecco's Modified Eagle Medium (DMEM) / Nutrient mixture F-12 Ham culture media, penicillin streptomycin sterile solution and L-cysteine were purchased from Sigma Aldrich. Oleic acid, acetic acid and phosphoric acid were purchased from Fischer Scientific. Triton® X-100 and hydrogen tetrachloroaurate (III) trihydrate ($HAuCl_4 \cdot 3H2O$) were purchased from Acros Organics. Fetal bovine serum (FBS) was purchased from Atlanta Biologicals. MTS assay dye was purchased from Promega.

Solutions were prepared according to standard laboratory procedures. All chemicals used were reagent grade and were used as supplied.

2.2. Synthesis of bifunctional Au-Fe_3O_4 nanoparticles. The synthesis of Au-Fe_3O_4 nanoparticles was carried out in air by simultaneous addition of $Fe(CO)_5$ and $HAuCl_4$ with excess oleylamine (OLAM) and oleic acid (OLAC). 5 mL Triton® X-100 was added to a three neck round bottom flask equipped with a magnetic stir bar and air condenser. The solution was heated to 85 ºC. 2.5 mM of $Fe(CO)_5$, 0.25 mM of $HAuCl_4$, 2.5 mM OLAC, and 2.5 mM of OLAM were injected in this hot solution. The temperature was then ramped to 300 ºC. Upon injection of the Au and Fe-precursors, the solution turned black with rapid evolution of gases. After 10 min the gases subsided and the black solution was allowed to reflux for 1 h. After 1 h, heating was stopped and the reaction was cooled to room temperature.

2.3. Purification of crude product. The product was isolated from the reaction mixture by washing and centrifugation at least 3-4 times with ethanol using ultrasonication to remove excess Triton® X-100 and any unreacted precursors. The powder collected at the bottom of the centrifuge tube was dried in air. The black powder obtained after drying was characterized further through powder X-ray diffraction (PXRD), scanning and transmission electron microscopy (SEM and TEM, respectively), energy dispersive spectroscopy (EDS), UV-Vis, Mössbauer and magnetometry studies. Millipore water was used throughout to disperse the nanoparticles as needed for characterization as well as further studies.

2.4. Characterization of bifunctional Au-Fe_3O_4 nanoparticles.

PXRD: As-synthesized nanoparticles was ground and used for PXRD, which was carried out on Philips Xpert diffractometer scanning from 5 º to 90 º.

TEM & SEM: TEM images were taken by using Tecnai F20 transmission electron microscope with FEG at an accelerating voltage of 200kV. A dual beam Helios 600 Nano was used for SEM and STEM studies. Samples for TEM and STEM studies were made by dispersing as-synthesized nanoparticles in ethanol by ultrasonication for 2 h and adding drops from the diluted dispersion on a carbon coated 300 mesh Cu grid followed by drying in air overnight.

Optical studies: The UV-vis absorption studies were carried out with Cary 50 UV-vis spectrophotometer.

Magnetic characterization: Temperature dependent magnetic moment at constant field and field dependent isothermal magnetization measurements were performed with SQUID (Superconducting quantum interference device) magnetometer. The powdered sample of a known mass (8.8 mg) was loaded in a gel cap, which was inserted into the magnetometer with the help of standard sample loader. Background signal was collected from the diamagnetic gel cap separately and subtracted from the sample signal. Zero field cooled (ZFC) data was collected after cooling down the sample under zero magnetic field, and them recording magnetization as a function of warming temperature under an applied field of 100 Oe. The field cooled data (FC) on the other hand, was collected by cooling down the sample under an applied magnetic field and simultaneously recording the sample magnetization as a function of decreasing temperature. The isothermal magnetization at various temperatures (5 K, 100 K and 300 K) was collected by varying applied magnetic field from -20000 Oe to 20000 Oe and recording the change in sample magnetization.

Mössbauer spectroscopy: The transmission ^{57}Fe Mössbauer spectrum of the powdered sample was recorded at room temperature using a gamma-ray source of ^{57}Co in a Rhodium matrix. The spectrum data was fitted using Lorentzian function in RECOIL software [35]. Isomer shifts and quadruple splitting are given with respect to α-Fe foil at 298 K.

2.5. Preparation of L-cysteine modified bifunctional Au-Fe_3O_4 nanoparticles.

Cysteine solution of concentration 0.5 mg/mL was prepared by dissolving 50 mg of L-cysteine in 100 mL Millipore water. 10 mL of this solution and 20mg of as-synthesized Au-Fe3O4 nanoparticles were taken into a flat-bottomed conical flask with glass stopper. The flask was sealed with parafilm and placed on an orbital shaker for 24hrs at 150 rpm. After incubation, the nanoparticles were separated by attraction to a magnet and 0.5 mL from the supernatant was taken for acid ninhydrin assay [36]. The magnetically separated nanoparticles were further dried and characterized by FTIR and Raman spectroscopic studies.

2.6. Characterization of L-cysteine modified bifunctional Au-Fe_3O_4 nanoparticles. IR spectra were acquired with a Thermo Nicolet Nexus 470 FTIR spectrometer. The functionalized nanoparticle powder was intimately mixed with dry KBr into a homogenous fine powder with a mortar-pestle. Pellets were made from this homogenized mixture by compression using Carver Press at 15000 psi. The spectra were collected over a range of 400 – 4000 cm^{-1}. Horiba Jobin Yvon Lab Raman ARAMIS model was used to perform Raman microspectroscopy on the functionalized nanoparticles. The laser used was He-Ne with a power of about 1.7 mW over a range of 100 – 2000 cm^{-1}. The spectra were iterated over an average of 25 scans.

2.7. Acid ninhydrin assay. Acid ninhydrin assay was performed according to the literature as an instant method of L-cysteine detection. The reaction mixture for standard containing 0.5 mL of L-cysteine solution (0 – 0.5 mg/mL), 0.5mL of acetic acid and 0.5mL of acid ninhydrin reagent was mixed thoroughly. The test tubes were covered with caps and heated in boiling water for 10 min. They were rapidly cooled under running tap water, and the contents were diluted to 5 mL using 95% ethanol. A blank containing only sample solution from the supernatant without L-cysteine was also prepared under the same conditions. The absorbance standard plot was calculated at 560 nm with Shimadzu UV 1700 spectrophotometer. Acid ninhydrin reagent was prepared by dissolving 250 mg of ninhydrin in a mixture of 6 mL of acetic acid and 4 mL of 0.6 M phosphoric acid. The reagent was stable for 2 weeks at 4 ºC.

2.8. Cell culture. CHO cells were cultured in Dulbecco's Modified Eagle Medium (DMEM) / Nutrient mixture F-12 Ham culture media supplemented with 10% fetal bovine serum (FBS) and 1% penicillin/streptomycin. Cell cultures were incubated at 37 ºC in a humidified atmosphere of 5% CO_2 and 95% air.

2.9. Cytotoxicity. Cell viability was assessed by the MTS assay (CellTiter 96® AQueous One Solution Cell Proliferation Assay), based on the conversion of a tetrazolium compound, 3-(4,5-dimethylthiazol-2 yl)-5-(3-carboxymethoxyphenyl)-2-(4-sulfophenyl)-2H tetrazolium (MTS), to a colored formazan product by living cells [37]. Absorbance was read by a microplate reader at 490 nm. The quantity of formazan product, as measured by the amount of absorbance, was directly proportional to the number of viable cells in the culture.

10,000 CHO cells were seeded in each well of 96-well plates. After 24 h, the medium was then discarded and replaced with serum free fresh medium containing the Au-Fe_3O_4 nanoparticles at different concentrations for 48 hr. CellTiter 96® AQueous One reagent (20 µl/well) was added to each well and the plate was incubated for 1.5 h at 37 ºC in a humidified atmosphere of 5% CO_2 and 95% air, and then centrifuged to get rid of nanoparticles. The MTS formazan product was measured by determining the absorbance of the supernatant (100 µL) at 490 nm using a 96-well plate reader (FLUOstar, BMG Labtechnologies, Durham, NC, USA). The relative cell viability (%) related to control wells containing culture medium without nanoparticles was calculated by $[A]_{test}/[A]_{control} \times 100$.

3. RESULTS AND DISCUSSION

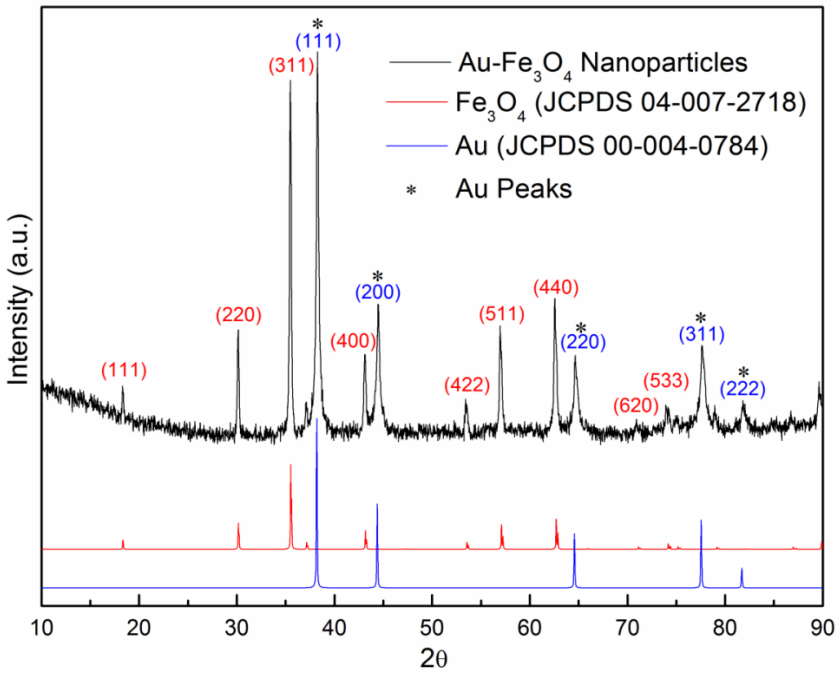

Figure 1. PXRD pattern of Au-Fe_3O_4 bifunctional nanoparticles synthesized at 300°C

Figure 1 shows the formation of highly crystalline Au-Fe_3O_4 nanoparticles confirmed by PXRD pattern, which corroborated very well with the standard patterns of Fe_3O_4 with inverse spinel structures(JCPDS 04-007-2718) and Au (JCPDS 00-004-0784). The PXRD pattern was very clean and did not show any impurity peaks corresponding to other iron oxide phases like Fe_2O_3 and FeOOH. From Schrerrer equation the size of these particles was calculated to be 75 nm with the Fe_3O_4 region being around 60 nm while the Au part

was around 15 nm in average [38]. The size of nanoparticles could be tuned by controlling the time at which $HAuCl_4$ was injected, presence of OLAM in the reaction mixture (excess OLAM led to bigger gold particles), reflux time and the $HAuCl_4/Fe_3O_4$ ratio. Specifically, injecting $Fe(CO)_5$ in large excess compared to $HAuCl_4$ (~20:1 Fe:Au molar ratio) led to overgrowth of Fe_3O_4 part while refluxing the reaction mixture for longer time resulted in agglomeration of Au-Fe_3O_4 particles. Presence of OLAM helps in reduction of Au^{+3} to Au^0 onto the Fe_3O_4 surface. The role of Triton® X-100 was more as a highly viscous solvent which inhibited overgrowth of the Fe_3O_4 part and changing the concentration of Triton® X-100 had very minimal effect on the morphology of the Au-Fe_3O_4 nanoparticles.

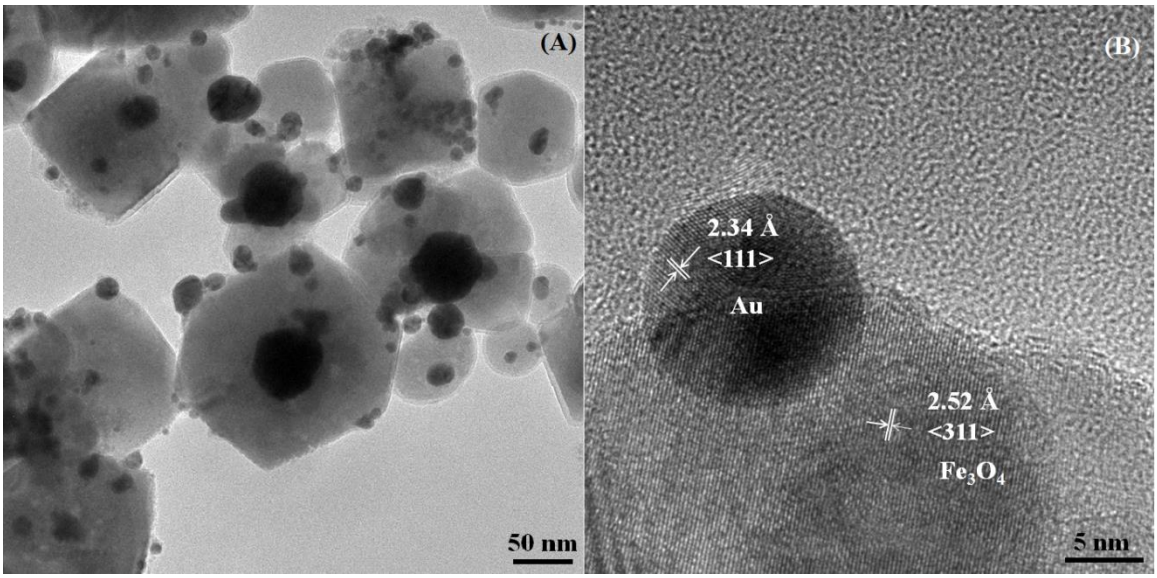

Figure 2. (A) TEM image of the bifunctional nanoparticles showing decoration of Fe_3O_4 with Au. (B) HRTEM showing the attachment of Au to Fe_3O_4 and the crystallinity of the individual regions. Lattice fringes from the Au and Fe_3O_4 regions corresponds to <111> and <311> planes, respectively.

The morphology and composition of the bifunctional nanoparticles were characterized by transmission electron microscopy (TEM) and scanning electron microscopy (SEM). Investigations from TEM and SEM showed a high yield of bifunctional nanoparticles in the product with uniform particle size distribution. Figure 2(A) shows a typical distribution of the Au-Fe_3O_4 nanoparticles where each Fe_3O_4 region is decorated with several Au dots. Typically the Fe_3O_4 regions (lighter contrast in the

images) were 80 nm while the Au part (darker contrast) was approximately 20 nm. Several wide area SEM images were obtained to calculate the average particles size. The size of the Au and Fe_3O_4 particles ranged from 5-20 nm and 50-80 nm, respectively, with average bifunctional particle size around 80 nm. This kind of morphology is slightly different than the dumbbell shaped particles and is closer to multifaceted Janus particles [39, 40]. This kind of morphology (Au-decorated Fe_3O_4) gives the added advantage that both Au and Fe_3O_4 functionalities are available for full utilization of their potential, while, several Au dots on the Fe_3O_4 host ensures that there are maximum number of spots for molecular recognition since Au-terminal acts as anchor for the aptamers used as targeting agents. Au-Fe_3O_4 nanoparticles were highly crystalline as revealed by the high resolution TEM (HRTEM) image shown in figure 2(B). The HRTEM image exhibited lattice fringes corresponding to (111) planes of Au and (311) lattice planes of Fe_3O_4. Through these HRTEM images we also looked in detail at the interfaces between the Au and Fe_3O_4 regions. The interface in these nanoparticles was very clean and well-defined with minimal mixing of the Au and Fe_3O_4 phases. There was no fuzziness or presence of any other crystalline phase at the interface. Interfacial surface can be very important in these superparamagnetic nanoparticles as depending on the composition on both sides of the interface they might lead to exchange bias magnetic interactions leading to interparticle interaction and ordering.

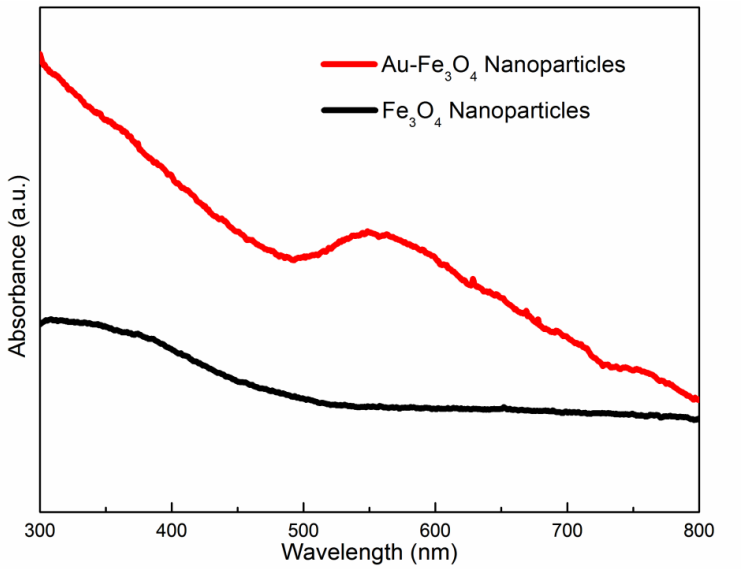

Figure 3. Absorption spectra of the bifunctional Au-Fe_3O_4 nanoparticles and Fe_3O_4 nanoparticles

Gold nanoparticles ranging in size from 5-20 nm are reported to show a plasmon resonance band at 520 nm. This phenomenon can be attributed to the resonance condition satisfied between the incoming light frequency and natural frequency of the surface electrons oscillating against the positive force of nuclei. The bifunctional Au-Fe_3O_4 nanoparticles reported here show red shift of plasmon resonance band due to the attachment of Au with Fe_3O_4 nanoparticles although the exact position of the absorption maxima varied with the gold particle size attached to Fe_3O_4 part. A typical spectrum exhibited that the Au-Fe_3O_4 nanoparticles in ethanol shows a plasmon resonance band ~540 nm (figure 3), which is shifted by ~20 nm from pure Au nanoparticles. This red shift can be accounted for the deficiency of electrons on Au due to the interaction with Fe_3O_4 [41, 42]. The absorption spectra collected from pure Fe_3O_4 nanoparticles did not show any peak in the 300 – 800 nm regions.

These bifunctional Au-Fe_3O_4 nanoparticles deserve a very careful magnetic characterization since *Magnetite* (Fe_3O_4) is one of the oldest and interesting magnetic materials known to the scientific community. Bulk magnetite is ferrimagnetic with Curie temperature around 858 K. In 1939, Verwey [43] observed first order transition on cooling below 120 K which resulted in increased resistivity and distortion of the cubic symmetry of magnetite. Charge ordering of different states of iron (Fe^{2+} and Fe^{3+}) on the octahedral sites in alternating layers was ascribed to be the reason for this transition [44]. The temperature below which this transition occurs is termed Verwey temperature (T_V). To better understand the magnetic properties of these gold-magnetite nanoparticles, we performed detailed magnetization measurements as a function of temperature and applied magnetic field. The magnetization behavior of the sample as a function of temperature was measured under ZFC and FC conditions under an applied magnetic field of 100 Oe are shown in figure 4(A). These nanoparticles show a clear Verwey transition at 120 K visibly prominent in the ZFC curve. For the superparamagnetic nanoparticles there are two basic criterions. First is that the magnetization as a function of H/T for non-interacting single domain particles must be fitted by *Langevin* equation (1) [27, 45] as shown below.

$$M = Mo\left[\coth\left(\frac{\mu H}{k_B T}\right) - \frac{1}{\left(\frac{\mu H}{k_B T}\right)}\right] \quad \ldots(1)$$

where M = magnetization, M_0 = saturation magnetization, H = applied magnetic moment, μ = magnetic moment, T = temperature and k_B = Boltzmann constant. The plot of M versus H/T at 5 K, 100 K and 300 K converge into a single universal curve and could be fitted using Langevin equation with R^2=0.9981 as shown in figure 4(B). Second condition for superparamagnetic particles is the anhysteretic nature of isothermal magnetization against applied magnetic field with zero coercivity, which is also temperature independent above blocking temperature (T_B).

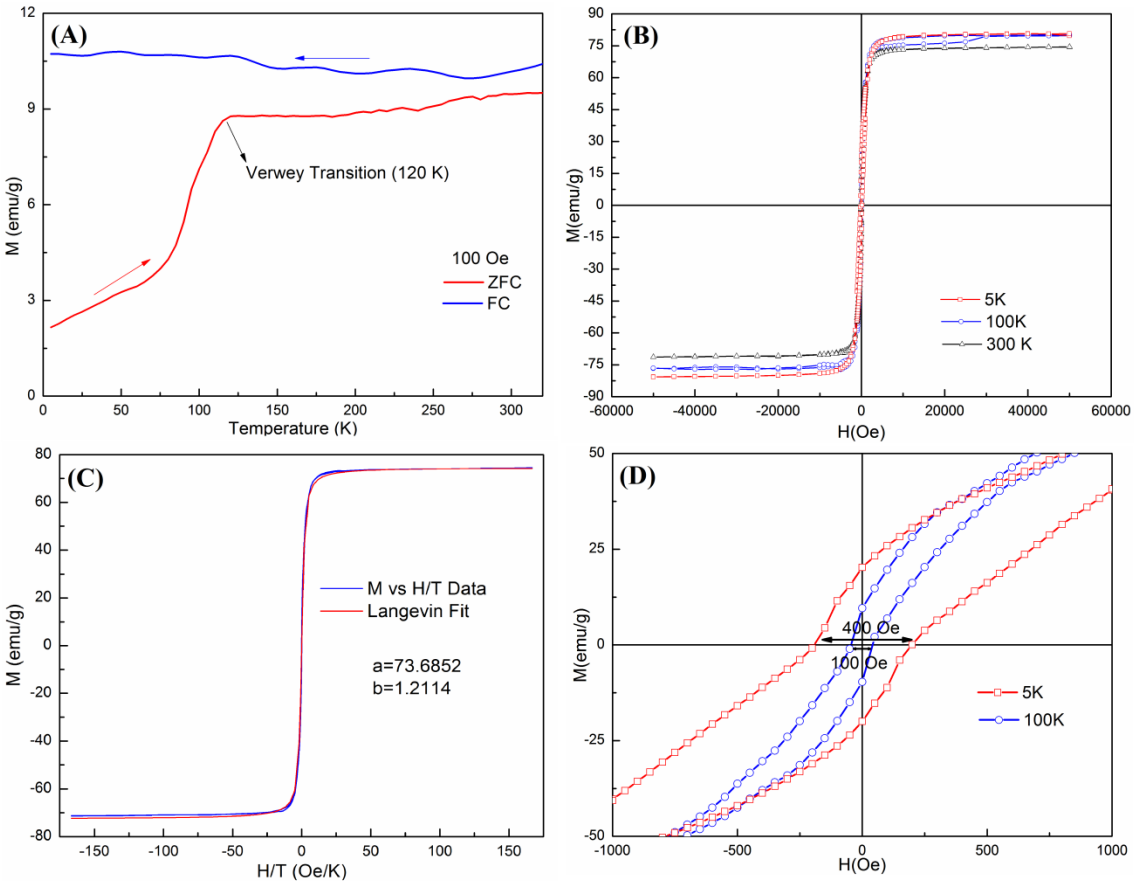

Figure 4. (A) ZFC and FC curves of the Au-Fe_3O_4 nanoparticles under an applied field of 100 Oe. (B) *M* vs *H* plots at 5 K, 100 K and 300 K. (C) The *Langevin* fit at 300 K. (D) *M* vs *H* plots at 5 and 100 K magnified to show the coercive fields.

Figure 4(C) shows the isothermal magnetization curves as a function of applied magnetic field at 5 K, 100 K and 300 K for the bifunctional nanoparticles. The presence of coercivity was very apparent at 5K and 100K. At 300 K on the other hand, the M vs H was anhysteretic in nature typical for a superparamagnetic nanoparticle, as shown in

figure 4D. This indicates that the Au-Fe_3O_4 nanoparticles were superparamagnetic at 300 K with T_B lying in between 100 – 300 K. Generally for magnetite nanoparticles, it is assumed that T_v is greater than blocking temperature with the exemption of any chain formation of the particles which is absent in our particles [46]. However, it is also known that for superparamagnetic nanoparticles the T_B increases with increasing particle size within the single domain range [27, 45]. For Fe_3O_4 nanoparticles it has been estimated that the maximum allowable size for single domain particle is ~120 nm [45]. The average size of Fe_3O_4 region in the Au-Fe_3O_4 ensemble was ~60 nm which indicates that these nanoparticle ensembles may be on the realm of single domain superparamagnetic behavior and multi-domain characteristics. Skumryev have recently shown that it is possible to beat the superparamagnetic limit by formation of exchange bias interactions [47] caused by several factors including magnetic coupling at the interface, uncompensated spins on the surface, as well as the presence of multiple interfaces in these composite magnetic nanoparticles [48]. Previously, Sun et al. have shown that higher T_B and higher coercivity could be obtained due to exchange bias in nanoflower-like Au-Fe_3O_4 nanoparticles [48]. According to the literature Fe_3O_4 nanoparticles with an average size in the range of 50 nm shows a T_B close to room temperature [49]. In the current case the anhysteretic nature of M vs H curve for the Au-Fe_3O_4 nanoparticle ensemble at 300 K along with the nature of the ZFC-FC curves indicate that the T_B is very close to room temperature. At 300 K the Au-Fe_3O_4 nanoparticle ensemble is right at the interface of superparamagnetic and ordered states thereby possessing high magnetic moment as well as the thermally activated spontaneous particle moment fluctuations. The coercivity observed at 5 K and 100 K might indicate that near the Verwey phase transition, changes in resistivity and distortion of symmetry may occur due to charge ordering. The saturation magnetization for these Au-Fe_3O_4 nanoparticles was 73.68 emu/g at 300 K which is almost 80% of the saturation magnetization of bulk magnetite (~92 emu/g) [50]. Such enhanced magnetic properties can be also attributed to the typical morphology of these Au-Fe_3O_4 nanoparticles where each Fe_3O_4 is decorated with several non-magnetic Au dots which can function as surface passivation agents thereby pushing the superparamagnetic limit. Additionally, if the nanoparticles are not absolutely immobilized and well separated, inter-particle interactions will influence the relaxation

and if the magnetic interaction energy exceeds the thermal energy, it will lead to a degree of ordering of the particle moments, resulting in behavior typically referred to as superferromagnetism [51]. These phenomena can give rise to higher saturation magnetization compared to bare Fe_3O_4 nanoparticles with smaller sizes.

The average particle volume of superparamagnetic nanoparticles could be also estimated using the following equations along with the Langevin equation (1).

$$y = a\left[\coth(bx) - \frac{1}{(bx)}\right] \quad \ldots(2)$$

where x = H/T; y = M; a = M_0 and b = μ/k_B.

Particle moment, $\mu = M_S\langle V\rangle$ …(3)

where M_S = saturation moment of Fe_3O_4 nanoparticles; and <V> = average particles volume.

The observed saturation moment of Fe_3O_4 is ~74 emu/g from the Langevin fit. Parameters a and b could be obtained from the Langevin fit of M vs H/T at 300 K and through proper substitution of these parameters in equation 3, the average particle volume can be calculated (the density of Fe_3O_4 was taken to be 5.197 g/cc corresponding to the literature). Assuming the particles were spherical, the average particle diameter obtained using this approach was approximately 58 nm. Since this approach only accounts for the superparamagnetic part in these bifunctional nanoparticles (i.e. Fe_3O_4 region), the overall size of the nanoparticles including the average diameter of the Au region (~20 nm) would be approximately 78 nm, which was close to the average particle size observed through STEM and TEM investigations (~80 nm).

These bifunctional nanoparticles were also characterized by Mössbauer spectroscopy. The Mössbauer spectrum collected from the as-synthesized nanoparticles ensemble at room temperature showed two sextets characteristic for A and B sites of iron in a stoichiometric inverse spinel crystal structure of Fe_3O_4 [52]. The two sextets with isomer shifts, quadruple splittings, quadrapole shifts and hyperfine field for one subspectra (0.66 mm/s, 3.11 mm/s, 0.005 mm/s, and 46 T, respectively) and the other (0.29 mm/s, 3.33 mm/s, 0 mm/s, and 49 T, respectively) relative to the α-Fe metal suggests the existence of Fe^{3+} in A site and the co-existence of Fe^{2+} and Fe^{3+} in B site (figure 5). The ratio between areas under the subspectra A and B is ~1.75 [53-56]. The slight broadening of peaks can be attributed to reduced size and polydispersity in these

nanoparticle ensembles. The observed Mössbauer spectra were very similar to the ones reported in the literature for Fe_3O_4 albeit with size ranges close to 50 – 100 nm [50]. It should be noted that two sets of sextet observed in Mössbauer spectra was more closely related to the ordered state rather than the superparamagnetic state for Fe_3O_4 nanoparticles. This also corroborates with our hypothesis that at 300 K the ensemble is on the cusp of superparamagnetic and ordered states. Typically, T_B is very dependent on the analysis method since the relaxation time for the moment fluctuation (τ_o) is dependent on the measurement time of the instrument (τ_m) as shown below in equation 4 [47].

$$\tau_m = \tau_0 \exp\left(\frac{KV}{k_B T}\right) \quad \ldots(4)$$

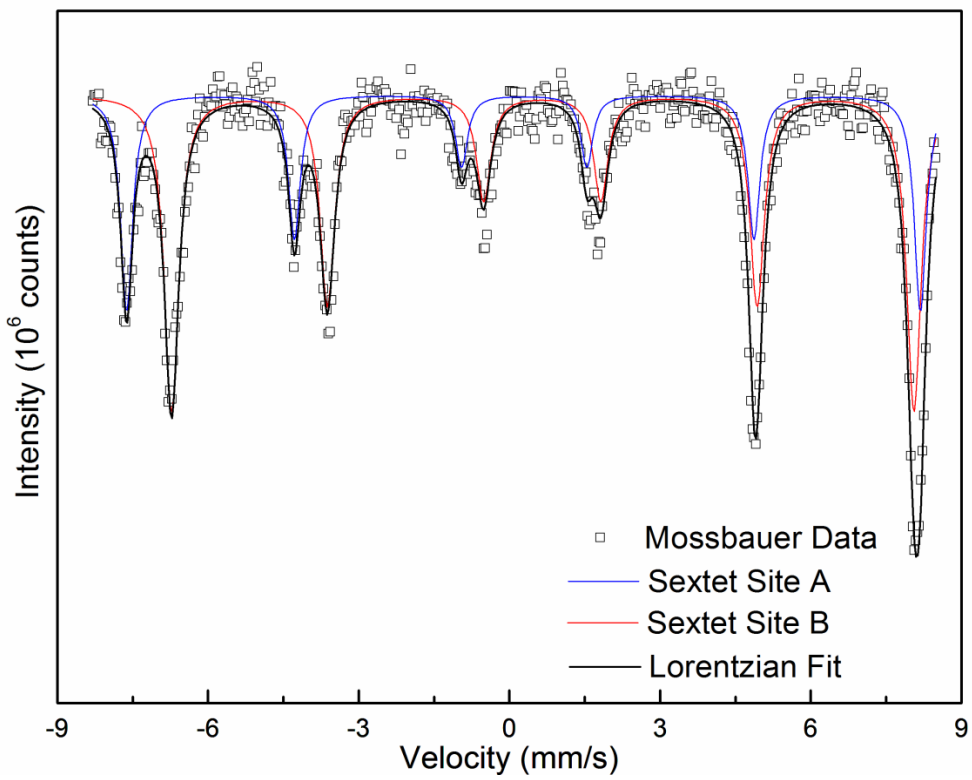

Figure 5. Mössbauer spectrum of Au-Fe_3O_4 nanoparticles collected at room temperature with zero magnetic field showing the two characteristic sextets corresponding to Fe^{3+} and Fe^{2+} states.

Since, γ-ray detection in Mössbauer spectroscopy is a comparatively fast technique (τ_o = 10^{-7} s), the T_B estimated from Mössbauer data is typically higher than that obtained from

magnetization studies. In general the T_B determined from these two techniques is related by the following equation 5 [47].

$$\frac{T_B(Mössbauer)}{T_B(Magnetometer)} \cong 5.5 \quad \ldots(5)$$

Hence, it can be concluded that at 300 K with respect to Mössbauer studies the Au-Fe_3O_4 ensembles still behaves as if it is in the ordered state (i.e. below T_B) while in magnetization studies under an applied magnetic field it behaves closer to a superparamagnet. The similarity between these spectra with that observed for bulk Fe_3O_4 also ruled out the presence of Fe in any other oxidation states.

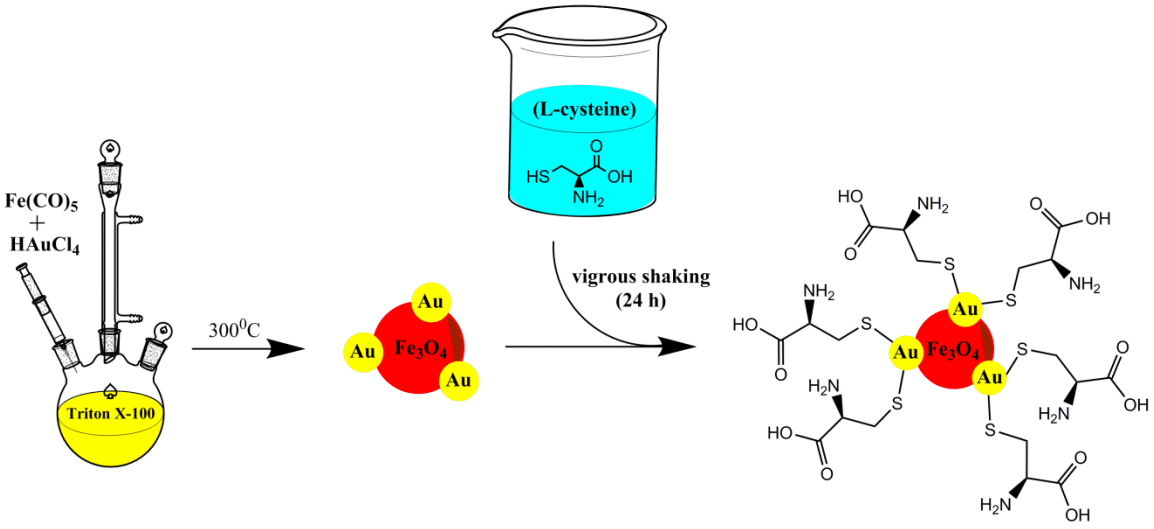

Figure 6. Scheme showing the functionalization of Au-Fe_3O_4 bifunctional nanoparticles by attachment of L-cysteine to the Au-terminal.

As mentioned previously, one of the most potentially transformative applications of these magnetic nanoparticles is in biomedical fields. Hence, to demonstrate the feasibility of using these bifunctional nanoparticles for biological applications, we functionalized the nanoparticles taking advantage of Au-thiol facile interactions to make these composite structures more biocompatible. In this regards, we have successfully attached L-cysteine to Au terminal of the bifunctional nanoparticles by the process described in the experimental section. The process for functionalization with L-cysteine and the expected morphology has been schematically shown in figure 6. Both qualitative (through FTIR and Raman) and quantitative (through acid ninhydrin assay) analysis of the L-cysteine-modified Au-Fe_3O_4 bifunctional nanoparticles were performed. Figure

7(A) shows the FTIR spectra of L-cysteine-modified Au-Fe_3O_4 bifunctional nanoparticles (curve 2) as compared with that of free L-cysteine (curve 1). While most of the bands assigned to cysteine were visible for both the samples, the absence of band at ~2551 cm^{-1} corresponding to the stretching vibration of S-H bond was prominent in the FTIR spectra of the cysteine functionalized nanoparticles as shown in curve b. This indicates breakage of the S-H bond on attachment of cysteine to the Au –terminal through S, and has been accepted as a signatory evidence for successful molecule attachment. [57-59]. Trans C-S stretching vibrational modes can be assigned to the presence of band at ~637 cm^{-1}. The band at ~3422 cm^{-1} can be assigned to N-H stretching vibrations [59], while bands in the range 1510 to 1680 cm^{-1} can be assigned to carbonyl and N-H stretching vibrations [60]. Detailed analysis of the FTIR spectra confirmed the attachment of L-cysteine to the Au-Fe_3O_4 bifunctional nanoparticles.

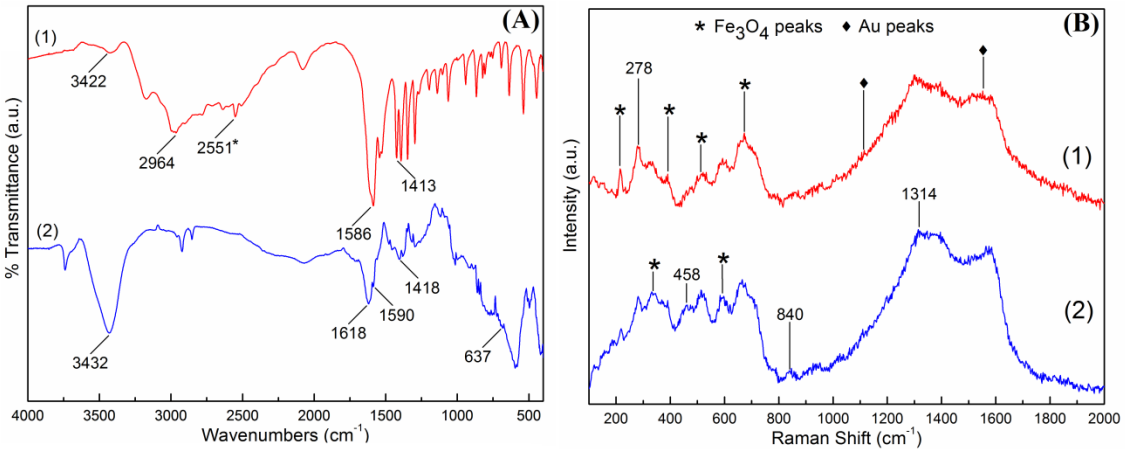

Figure 7. (A) FTIR spectra of (1) pure L-cysteine and (2) L-cysteine modified-bifunctional Au-Fe_3O_4 nanoparticles (B) Raman spectra of (1) bifunctional Au-Fe_3O_4 nanoparticles and (2) L-cysteine modified Au-Fe_3O_4 nanoparticles.

From a purely group theory-based analysis, Fe_3O_4 should exhibit 14 Raman active modes ($3A_1+3E+8T_2$). But, experimentally all modes cannot be detected due to the mutual exclusion of vibrational modes caused by the presence of inversion center of symmetry. Additional peaks may be present if the sample has any defects or vacancies. Group theory analysis doesn't account for these factors [61]. In our study, we observed six peaks corresponding to Fe_3O_4 at 215, 329, 393, 516, 597, 672 cm^{-1} and two peaks

corresponding to Au at 1113 and 1552 cm^{-1} as shown in figure 7(B). Curve (1) corresponds to as-synthesized Au-Fe_3O_4 nanoparticles while curve (2) corresponds to L-cysteine attached Au-Fe_3O_4 nanoparticles. Results were compared to the previously published data on magnetite [62-65]. According to the literature, peaks at 215, 516, 597 cm^{-1} correspond to T_{2g}, 329 cm^{-1} corresponds to E_g and 672 cm^{-1} corresponds to A_{1g} mode. Peaks at 278 and 1314 cm^{-1} indicate the presence of defect or transformation of the magnetite region to hematite which could be a consequence of the power of the laser used (1.7 mW) [40]. The peak at 393 cm^{-1} corresponds to the surface magnon excitation [66]. Peaks at 458 and 840 cm^{-1} in curve (2) of figure 7(B) correspond to the (C-C-N) bending and (O-C-O) wagging from the L-cysteine attached to the nanoparticles [67]. Peaks corresponding to gold at 1113 and 1552 cm^{-1} maybe damped by the attachment of gold in curve (2) of figure 7(B) [68].

While qualitative analysis showed that the Au-Fe_3O_4 nanoparticles could be actually functionalized with L-cysteine attachment, the quantitative analysis was performed by estimating the amount of leftover cysteine in the supernatant through acid ninhydrin assay, an instant spectrophotometric method [58]. In this assay, the supernatant was analyzed for L-cysteine after magnetically separating the nanoparticles from the L-cysteine solution. This indirect approach was employed due to presence of Au-Fe_3O_4 nanoparticles in the product, where Au exhibits unique optical properties, which could interfere with the absorbance readings. After 24 h vigorous shaking of nanoparticles in L-cysteine solution, the functionalized nanoparticles were separated using a magnet since the nanoparticles were quickly attracted to the magnet as shown in figure 8(A). Then acid ninhydrin reagent was added to a portion of the supernatant and was kept in boiling water bath for 10 min. Figures 8(B) and 8(C) show the color change in the reaction solution after boiling. Figure 8(D) shows the standard curve of absorbance versus L-cysteine concentration (in mg/mL). From an initial concentration of 10 mg L-cysteine, 4.53 mg of L-cysteine was found to be in the supernatant (i.e. unattached to the nanoparticles).

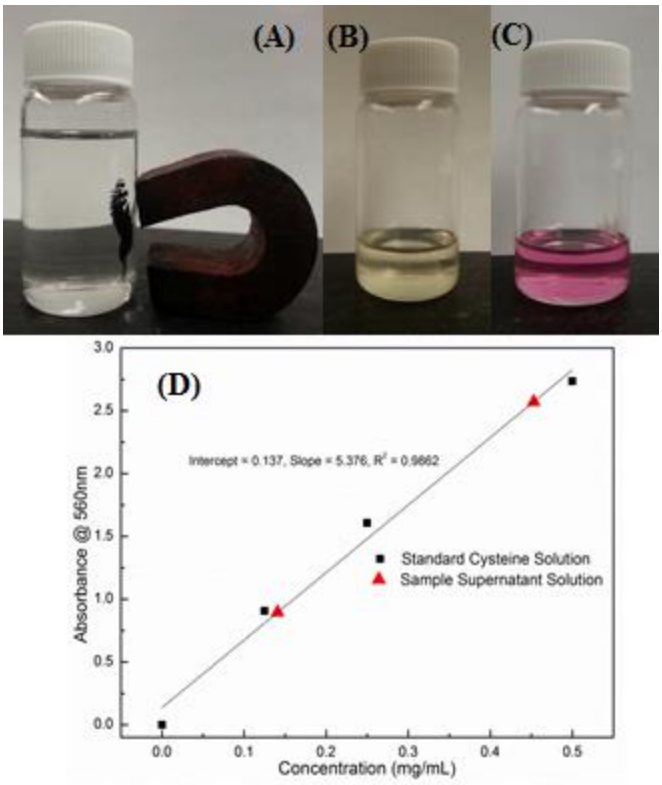

Figure 8. (A) Magnetic separation of the nanoparticles from the L-cysteine solution. (B) Color of supernatant after adding acid ninhydrin and (C) after heating in water bath for 15 minutes. (D) Standard curve of absorbance versus L-cysteine concentration.

Assuming 100% of L-cysteine activity, the loading capacity of the bifunctional nanoparticles used in the study is approximately 1 mg of L-cysteine per 4 mg of nanoparticles. We are presently trying to attach various other biomolecules to gain a better insight into the loading capacity of these bifunctional nanoparticles. Au-Fe_3O_4 nanoparticles are intended to be applied for magnetic fluid hyperthermia and delivery of biomolecules. Hence the cytotoxicity of these nanoparticles was also evaluated. For this study, the cell viability of CHO cells was evaluated after 48 h incubation at various increasing concentration of nanoparticles ranging from 0.1 – 1 mg/ml by MTS assay. The nanoparticles didn't show any sign of cytotoxicity even at 1 mg/mL (figure 9). The results obtained corroborates well with polymer coated magnetite nanoparticles and other morphologies [69-73].

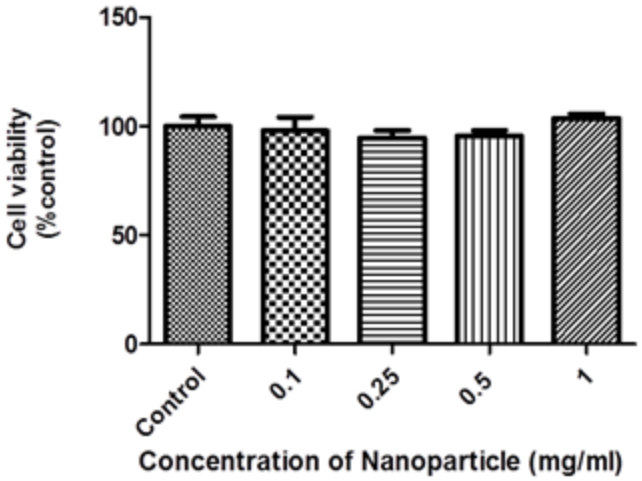

Figure 9. Cytotoxicity of Au-Fe_3O_4 nanoparticles at various concentrations for CHO cells after 48 h incubation.

4. CONCLUSION

We have successfully synthesized optically active superparamagnetic Au-Fe_3O_4 bifunctional nanoparticles using a simple one-pot synthesis method based on hot inject precipitation techniques. The morphology of the nanoparticles consisted of Fe_3O_4 (~70 nm) host decorated with several Au dots (~20 nm) (scheme 1). This kind of morphology would be very attractive for *theranostic* applications since they provide maximum points of attachment for aptamers and other cell recognition agents, while maintaining the pristine functionality of both the regions. The superparamagnetic nature of these nanoparticles was confirmed by the anhysteretic nature of the isothermal magnetization plot at 300 K. These Au-Fe_3O_4 nanoparticles could be functionalized with L-cysteine. The cell viability studies of these nanoparticles revealed their very low toxicity to CHO cells even at very high loading. These studies indicate that such decorated Au-Fe_3O_4 nanoparticles would be ideal candidates as magnetic fluid hyperthermia agents.

5. ACKNOWLEDGMENTS

The authors would like to acknowledge the Materials Research Center, for equipment usage and Dr. Kartik C. Ghosh for magnetic characterization.

6. REFERENCES

[1] Sotiriou G A 2013 Biomedical applications of multifunctional plasmonic nanoparticles WIREs Nanomed Nanobiotechnol 5 19-30

[2] Zeng H and Sun S 2008 Syntheses, Properties, and Potential Applications of Multicomponent Magnetic Nanoparticles Adv. Funct. Mater. 18 391-400

[3] Kim J, Piao Y and Hyeon T 2009 Multifunctional nanostructured materials for multimodal imaging, and simultaneous imaging and therapy Chem. Soc. Rev. 38 372-90

[4] Yue X-L, Ma F and Dai Z-F 2014 Multifunctional magnetic nanoparticles for magnetic resonance image-guided photothermal therapy for cancer Chin. Phys. B 23 044301

[5] Yan K, Li P, Zhu H, Zhou Y, Ding J, Shen J, Li Z, Xu Z and Chu P K 2013 Recent advances in multifunctional magnetic nanoparticles and applications to biomedical diagnosis and treatment RSC Adv. 3 10598-618

[6] Hao R, Xing R, Xu Z, Hou Y, Gao S and Sun S 2010 Synthesis, Functionalization, and Biomedical Applications of Multifunctional Magnetic Nanoparticles Adv. Mater. 22 2729-42

[7] Sotiriou G A, Starsich F, Dasargyri A, Wurnig M C, Krumeich F, Boss A, Leroux J-C and Pratsinis S E 2014 Photothermal Killing of Cancer Cells by the Controlled Plasmonic Coupling of Silica-Coated Au/Fe2O3 Nanoaggregates Adv. Funct. Mater. 24 2818-27

[8] Kim J, Kim H S, Lee N, Kim T, Kim H, Yu T, Song I C, Moon W K and Hyeon T 2008 Multifunctional Uniform Nanoparticles Composed of a Magnetite Nanocrystal Core and a Mesoporous Silica Shell for Magnetic Resonance and Fluorescence Imaging and for Drug Delivery Angew. Chem. Int. Ed. 47 8438-41

[9] McCarthy J R and Weissleder R 2008 Multifunctional magnetic nanoparticles for targeted imaging and therapy Adv. Drug Deliv. Rev.60 1241-51

[10] Huh Y-M, Jun Y-w, Song H-T, Kim S, Choi J-s, Lee J-H, Yoon S, Kim K-S, Shin J-S, Suh J-S and Cheon J 2005 In Vivo Magnetic Resonance Detection of Cancer by Using Multifunctional Magnetic Nanocrystals J. Am. Chem. Soc. 127 12387-91

[11] Fang C and Zhang M 2009 Multifunctional magnetic nanoparticles for medical imaging applications J. Mater. Chem. 19 6258-66

[12] Di Corato R, Bigall N C, Ragusa A, Dorfs D, Genovese A, Marotta R, Manna L and Pellegrino T 2011 Multifunctional Nanobeads Based on Quantum Dots and Magnetic Nanoparticles: Synthesis and Cancer Cell Targeting and Sorting ACS Nano 5 1109-21

[13] Bao G, Mitragotri S and Tong S 2013 Multifunctional Nanoparticles for Drug Delivery and Molecular Imaging Annu. Rev.Biomed. Eng. 15 253-82

[14] Bhaskar S, Tian F, Stoeger T, Kreyling W, de la Fuente J M, Grazu V, Borm P, Estrada G, Ntziachristos V and Razansky D 2010 Multifunctional Nanocarriers for diagnostics, drug delivery and targeted treatment across blood-brain barrier: perspectives on tracking and neuroimaging Part. Fibre Toxicol. 7 3

[15] Gao J, Gu H and Xu B 2009 Multifunctional magnetic nanoparticles: design, synthesis, and biomedical applications Acc. Chem. Res. 42 1097-107

[16] Daniel M-C and Astruc D 2004 Gold Nanoparticles: Assembly, Supramolecular Chemistry, Quantum-Size-Related Properties, and Applications toward Biology,Catalysis, and Nanotechnology Chem. Rev. 104 293-346

[17] Sperling R A, Gil P R, Zhang F, Zanella M and Parak W J 2008 Biological applications of gold nanoparticles Chem. Soc. Rev. 37 1896-908

[18] Ghosh P, Han G, De M, Kim C K and Rotello V M 2008 Gold nanoparticles in delivery applications Adv. Drug Deliv. Rev. 60 1307-15

[19] El-Sayed I H, Huang X and El-Sayed M A 2006 Selective laser photo-thermal therapy of epithelial carcinoma using anti-EGFR antibody conjugated gold nanoparticles Cancer Lett. 239 129-35

[20] Gupta A K and Gupta M 2005 Synthesis and surface engineering of iron oxide nanoparticles for biomedical applications Biomaterials 26 3995-4021

[21] Laurent S, Dutz S, Häfeli U O and Mahmoudi M 2011 Magnetic fluid hyperthermia: Focus on superparamagnetic iron oxide nanoparticles Adv. Colloid Interface Sci. 166 8-23

[22] Laurent S, Forge D, Port M, Roch A, Robic C, Vander Elst L and Muller R N 2008 Magnetic Iron Oxide Nanoparticles: Synthesis, Stabilization, Vectorization, Physicochemical Characterizations, and Biological Applications Chem. Rev. 108 2064-110

[23] Qiao R, Yang C and Gao M 2009 Superparamagnetic iron oxide nanoparticles: from preparations to in vivo MRI applications J. Mater. Chem. 19 6274-93

[24] Lewin M, Carlesso N, Tung C-H, Tang X-W, Cory D, Scadden D T and Weissleder R 2000 Tat peptide-derivatized magnetic nanoparticles allow in vivo tracking and recovery of progenitor cells Nature Biotechnol. 18 410-4

[25] Weissleder R, Moore A, Mahmood U, Bhorade R, Benveniste H, Chiocca E A and Basilion J P 2000 In vivo magnetic resonance imaging of transgene expression Nature Med. 6 351-4

[26] Zhao M, Beauregard D A, Loizou L, Daveletov B and Brindle K M 2001 Non-invasive detection of apoptosis using magnetic resonance imaging and a targeted contrast agent Nature Med. 7 1241-4

[27] Coey J M D 2010 Magnetism and Magnetic Materials (Cambridge University Press) p264

[28] Bao J, Chen W, Liu T, Zhu Y, Jin P, Wang L, Liu J, Wei Y and Li Y 2007 Bifunctional Au-Fe3O4 Nanoparticles for Protein Separation ACS Nano 1 293-8
[29] Yu H, Chen M, Rice P M, Wang S X, White R L and Sun S 2005 Dumbbell-like Bifunctional Au-Fe3O4particles Nano Lett. 5 379-82

[30] Liang C-H, Wang C-C, Lin Y-C, Chen C-H, Wong C-H and Wu C-Y 2009 Iron Oxide/Gold Core/Shell Nanoparticles for Ultrasensitive Detection of Carbohydrate-Protein Interactions Anal. Chem. 81 7750-6

[31] Xu Z, Hou Y and Sun S 2007 Magnetic Core/Shell Fe3O4/Au and Fe3O4/Au/Ag Nanoparticles with Tunable Plasmonic Properties J. Am. Chem. Soc. 129 8698-9

[32] Shevchenko E V, Bodnarchuk M I, Kovalenko M V, Talapin D V, Smith R K, Aloni S, Heiss W and Alivisatos A P 2008 Gold/Iron Oxide Core/Hollow-Shell Nanoparticles Adv. Mater. 20 4323-9

[33] Ji X, Shao R, Elliott A M, Stafford R J, Esparza-Coss E, Bankson J A, Liang G, Luo Z-P, Park K, Markert J T and Li C 2007 Bifunctional Gold Nanoshells with a Superparamagnetic Iron Oxide-Silica Core Suitable for Both MR Imaging and Photothermal Therapy J. Phy. Chem. C 111 6245-51

[34] Wang L, Luo J, Maye M M, Fan Q, Rendeng Q, Engelhard M H, Wang C, Lin Y and Zhong C-J 2005 Iron oxide–gold core–shell nanoparticles and thin film assembly J. Mater. Chem. 15 1821-32

[35] Vandenberghe R E, Grave E and Bakker P M A 1994 On the methodology of the analysis of Mössbauer spectra Hyperfine Interact. 83 29-49

[36] Gaitonde M K 1967 A Spectrophotometric Method for the Direct Determination of Cysteine in the Presence of Other Naturally Occurring Amino Acids Biochem. J. 104 627-33

[37] Cory AH, Owen TC, Barltrop JA, Cory JG 1991 Use of an aqueous soluble tetrazolium/formazan assay for cell growth assays in culture Cancer Comm. 3 207–12.

[38] Patterson A 1939 The Scherrer Formula for X-Ray Particle Size Determination Phys. Rev. 56 978-82

[39] Lattuada M and Hatton T A 2011 Synthesis, properties and applications of Janus nanoparticles Nano Today 6 286-308

[40] Perro A, Reculusa S, Ravaine S, Bourgeat-Lami E and Duguet E 2005 Design and synthesis of Janus micro- and nanoparticles J. Mater. Chem. 15 3745-60

[41] Haiss W, Thanh N T K, Aveyard J and Fernig D G 2007 Determination of Size and Concentration of Gold Nanoparticles from UV-Vis Spectra Anal. Chem. 79 4215-21

[42] Link S and El-Sayed M A 1999 Size and Temperature Dependence of the Plasmon Absorption of Colloidal Gold Nanoparticles J. Phy. Chem. B 103 4212-7

[43] Verwey E J W 1939 Electronic conduction of magnetite and its transition point at low temperatures Nature 144 327-8

[44] Wang J, Chen Q, Li X, Shi L, Peng Z and Zeng C 2004 Disappearing of the Verwey transition in magnetite nanoparticles synthesized under a magnetic field: implications for the origin of charge ordering Chem. Phys. Lett. 390 55-8

[46] Prozorov R, Prozorov T, Mallapragada S, Narasimhan B, Williams T and Bazylinski D 2007 Magnetic irreversibility and the Verwey transition in nanocrystalline bacterial magnetite Phys. Rev. B 76 054406

[47] Skumryev V, Stoyanov S, Zhang Y, Hadjipanayis G, Givord D and Nogues J 2003 Beating the superparamagnetic limit with exchange bias Nature 423 850-3

[48] Chandra S, Huls N A, Phan M H, Srinath S, Garcia M A, Lee Y, Wang C, Sun S, Iglesias O and Srikanth H 2014 Exchange bias effect in Au-Fe3O4 nanocomposites Nanotechnology 25 055702

[49] Goya G F, Berquó T S, Fonseca F C and Morales M P 2003 Static and dynamic magnetic properties of spherical magnetite nanoparticles J. Appl. Phys. 94 3520-8

[50] Roca A G, Morales M P, O'Grady K and Serna C J 2006 Structural and magnetic properties of uniform magnetite nanoparticles prepared by high temperature decomposition of organic precursors Nanotechnology 17 2783-8

[51] Morup, S. Superferromagnetic nanostructures Hyperfine Interactions, 1994, 90, 171-185

[52] O'Neill H S C and Dollase W A 1994 Crystal structures and cation distributions in simple spinels from powder XRD structural refinements: MgCr2O4, ZnCr2O4, Fe3O4

and the temperature dependence of the cation distribution in ZnAl2O4 Phys. Chem. Minerals 20 541-55

[53] Oh S J, Cook D C and Townsend H E 1998 Characterization of iron oxides commonly formed as corrosion products of steel Hyperfine Interact. 112 59-66

[54] Woo K, Hong J, Choi S, Lee H-W, Ahn J-P, Kim C S and Lee S W 2004 Easy Synthesis and Magnetic Properties of Iron Oxide Nanoparticles Chem. Mater. 16 2814-8

[55] Vandenberghe R E, Barrero C A, Costa G M d, Sana E V and Grave E D 2000 M¨ossbauer characterization of iron oxides and (oxy)hydroxides: the present state of the art Hyperfine Interact. 126 247-59

[56] Kumar R V, Koltypin Y, Xu X N, Yeshurun Y, Gedanken A and Felner I 2001 Fabrication of magnetite nanorods by ultrasound irradiation J. Appl. Phys. 89 6324-8

[57] Gao W, Ji L, Li L, Cui G, Xu K, Li P and Tang B 2012 Bifunctional combined Au-Fe(2)O(3) nanoparticles for induction of cancer cell-specific apoptosis and real-time imaging Biomaterials 33 3710-8

[58] Lo C K, Xiao D and Choi M M F 2007 Homocysteine-protected gold-coated magnetic nanoparticles: synthesis and characterization J. Mater. Chem. 17 2418-27

[59] Kumar A, Mandal S, Selvakannan P R, Pasricha R, Mandale A B and Sastry M 2003 Investigation into the interaction between surface-bound alkylamines and gold nanoparticles Langmuir 19 6277-82

[60] Shankar S S, Ahmad A, Pasricha R, Khan M I, Kumar R and Sastry M 2004 Immobilization of biogenic gold nanoparticles in thermally evaporated fatty acid and amine thin films J. Colloid Interface Sci. 274 69-75

[61] Wang Z, Lazor P, Saxena S K and O'Neill H S C 2002 High pressure Raman spectroscopy of ferrite MgFe2O4 Mater. Res. Bull. 37 1589-602

[62] Mandal M, Kundu S, Ghosh S K, Panigrahi S, Sau T K, Yusuf S M and Pal T 2005 Magnetite nanoparticles with tunable gold or silver shell J. Colloid Interface Sci. 286 187-94

[63] Faria D L A d, Silva S V and Oliveira M T d 1997 Raman Microspectroscopy of Some Iron Oxides and Oxyhydroxides J. Raman Spectrosc. 28 873-8

[64] Thibeau R J, Brown C W and Heidersbach R H 1978 Raman spectra of possible corrosion products of iron Appl. Spectrosc. 32 532-5

[65] Dunnwald J and Otta A 1989 An investigation of phase transitions in rust layers using Raman spectroscopy Corros. Sci. 29 1167-76

[66] Whangbo M-H, Koo H-J and Dai D 2003 Spin exchange interactions and magnetic structures of extended magnetic solids with localized spins: theoretical descriptions on formal, quantitative and qualitative levels J. Solid State Chem. 176 417-81

[67] Pawlukojc A, Leciejewicz J, Ramirez-Cuesta A J and Nowicka-Scheibe J 2005 l-Cysteine: Neutron spectroscopy, Raman, IR and ab initio study Spectrochim. Acta. Part A 61 2474-81

[68] Park H-Y, Schadt M J, Wang L, Lim I-I S, Njoki P N, Kim S H, Jang M-Y, Luo J and Zhong C-J 2007 Fabrication of Magnetic Core@Shell Fe Oxide@Au Nanoparticles for Interfacial Bioactivity and Bio-separation Langmuir 23 9050-6

[69] Salado J, Insausti M, Lezama L, Gil de Muro I, Moros M, Pelaz B, Grazu V, de la Fuente J M and Rojo T 2012 Functionalized Fe(3)O(4)@Au superparamagnetic nanoparticles: in vitro bioactivity Nanotechnology 23 315102

[70] Liong M, Lu J, Kovochich M, Xia T, Ruehm S G, Nel A E, Tamanoi F and Zink J I 2008 Multifunctional inorganic nanoparticles for imaging, targeting, and drug delivery ACS Nano 2 889-96

[71] Berry C C, Wells S, Charles S, Aitchison G and Curtis A S 2004 Cell response to dextran-derivatised iron oxide nanoparticles post internalisation Biomaterials 25 5405-13

[72] Yu W W, Chang E, Sayes C M, Drezek R and Colvin V L 2006 Aqueous dispersion of monodisperse magnetic iron oxide nanocrystals through phase transfer Nanotechnology 17 4483-7

[73] Fuente J M d l, Berry C C, Riehle M O and Curtis A S G 2006 Nanoparticle targeting at cells Langmuir 22 3286-93

SECTION

2. CONCLUSION AND FUTURE WORK

Optically active superparamagnetic gold-magnetite nanoparticles were synthesized using one pot hot injection precipitation method. The synthesis involved using $Fe(CO)_5$ as iron precursor and $HAuCl_4$ as gold precursor in presence of oleylamine and oleic acid. Oleylamine helps in reducing Au^{3+} to Au^0 seeds which simultaneously oxidizes Fe(0) to form Au-Fe_3O_4 bifunctional nanoparticles. Triton® X-100 was employed as a highly viscous solvent to prevent agglomeration of Fe_3O_4 nanoparticles. The morphology of the nanoparticles consisted of magnetite (~70 nm) part with gold dots (~20 nm). The superparamagnetic nature was confirmed by the anhysteretic nature of the isothermal plot at 300 K. The observed magnetization was approximately 74 emu/g which is significantly higher than previously reported values. By attaining high magnetization saturation, the patient need not be exposed to high magnetic fields for treatment. The pXRD pattern also didn't show any peaks corresponding to maghemite or iron oxyhydroxide. The toxicity of the nanoparticles was evaluated using MTS assay on CHO cells. They showed no significant toxic effect on CHO cells up to 48 hours.

L-cysteine was attached to these nanoparticles and was characterized qualitatively and quantitatively. Results showed that the loading capacity of the nanoparticles was 1 mg of L-cysteine per 4 mg of nanoparticles. The methods adopted in this thesis serve as facile and feasible method for synthesis of gold nanoparticles and their biomolecule conjugation through the gold terminal. The L-cysteine attached nanoparticles couldn't be dispersed in water. Future steps, would be to conjugate (-)-EGCG (epigallocatechin gallate) to these nanoparticles for specific binding to tumor cells.

Epigallocatechin gallate is the most abundant catechin in tea and is a potential antioxidant that has many therapeutic applications. Recent research shows that EGCG may be useful in preventing or treating various gastrointestinal, prostrate and other cancers. Initial studies show that the (-)-EGCG conjugated nanoparticles can be water dispersed. Figure 3.1 illustrate the attachment of EGCG to gold-magnetite nanoparticles.

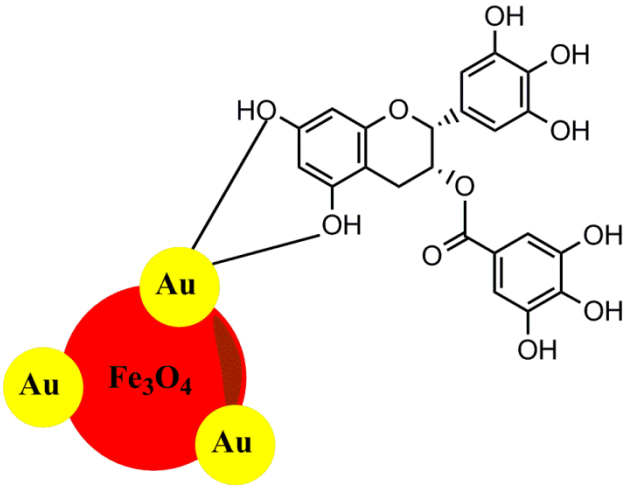

Figure 2.1. Schematic representation of gold magnetite nanoparticle conjugation with EGCG

These studies indicate gold magnetite nanoparticle-biomolecule conjugate would be ideal candidate as magnetic fluid hyperthermia agents.

BIBLIOGRAPHY

1. M-C. Daniel and D. Astruc, "Gold Nanoparticles: Assembly, Supramolecular Chemistry, Quantum-Size-Related Properties, and Applications toward Biology, Catalysis, and Nanotechnology," *Chemical Reviews*, Vol. 104, No. 1, Pp. 293-346 (2004).

2. A.P. Alivisatos, "Semiconductor Clusters, Nanocrystals, and Quantum Dots," *Science*, Vol. 271, No.5251, Pp. 933-7 (1996).

3. D.L. Fedlheim and C.A. Foss, *Metal nanoparticles: synthesis, characterizations, and applications*, CRC Press (2001).

4. K.A. Willets and R.P.Van Duyne, "Localized Surface Plasmon Resonance Spectroscopy and Sensing," *Annual Reviews of Physical Chemistry*, Vol. 58, Pp. 267-97 (2007).

5. H.C. van de Hulst, *Light Scattering by Small Metal Particles*, Wiley: New York (1957).

6. G. Mie, "Beiträge zur Optik Trüber Medien, Speziell Kolloidaler Metallösungen," *Annalen der Physik*, Vol. 330, No. 3, Pp. 377-445 (1908).

7. K.L. Kelly, E. Coronado, L.L. Zhao and G.C. Schatz, "The Optical Properties of Metal Nanoparticles: The Influence of Size, Shape, and Dielectric Environment," *The Journal of Physical Chemistry B*, Vol. 107, No. 3, Pp. 668-77 (2003).

8. S. Eustis and M.A. El-Sayed, "Why gold nanoparticles are more precious than pretty gold: Noble metal surface plasmon resonance and its enhancement of the radiative and nonradiative properties of nanocrystals of different shapes," *Chemical Society Reviews*, Vol. 35, No. 3, Pp. 209-17 (2006).

9. G. Schmid, "Large clusters and colloids. Metals in the embryonic state," *Chemical Reviews*, Vol. 92, No. 8, Pp. 1709-27 (1992).

10. M. Brust, M. Walker, D. Bethell, D.J. Schiffrin and R. Whyman, "Synthesis of thiolderivatized gold nanoparticles in a 2-phase liquid–liquid system," *Journal of the Chemical Society, Chemical communications*, No. 7, Pp. 801–802 (1994).

11. A.C. Templeton, W.P. Wuelfing and R.W. Murray, "Monolayer-Protected Cluster Molecules," *Accounts of Chemical Research*, Vol. 33, No. 1, Pp. 27-36 (2000).

12. J. Turkevich, P.C. Stevenson and J. Hillier, "A study of the nucleation and growth processes in the synthesis of colloidal gold," *Discussions of Faraday Society*, No. 11, Pp. 55-75 (1951).

13. R.A. Sperling, P.R. Gil, F. Zhang, M. Zanella and W.J. Parak, "Biological applications of gold nanoparticles," *Chemical Society Reviews*, Vol. 37, No. 9, Pp. 1896-1908 (2008).

14. P. Ghosh, G. Han, M. De, C.K. Kim and V.M. Rotello, "Gold nanoparticles in delivery applications," *Advanced Drug Delivery Reviews*, Vol. 60, No. 11, Pp. 1307-1315 (2008).

15. K. Saha, S.S. Agasti, C. Kim, X. Li and V.M. Rotello, "Gold Nanoparticles in Chemical and Biological Sensing," *Chemical Reviews*, Vol. 112, No. 5, Pp. 2739-79 (2012).

16. C.A. Mirkin, R.L. Letsinger, R.C. Mucic and J.J. Storhoff, "A DNA-based method for rationally assembling nanoparticles into macroscopic materials," *Nature*, Vol. 382, Pp. 607–609 (1996).

17. R. Elghanian, J.J. Storhoff, R.C. Mucic, R.L. Letsinger and C.A. Mirkin, "Selective Colorimetric Detection of Polynucleotides Based on the Distance-Dependent Optical Properties of Gold Nanoparticles," *Science*, Vol. 277, No. 5329, Pp. 1078-81 (1997).

18. M-R. Choi, K.J. Stanton-Maxey, J.K. Stanley, C.S. Levin, R. Bardhan, D. Akin, S. Badve, J. Sturgis, J.P. Robinson, R. Bashir, N.J. Halas and S.E. Clare, "A Cellular Trojan Horse for Delivery of Therapeutic Nanoparticles into Tumors," *Nano Letters*, Vol. 7, No. 12, Pp. 3759-65 (2007).

19. T.B. Huff, L. Tong, Y. Zhao, M.N. Hansen, J-X. Cheng and A. Wei, "Hyperthermic effects of gold nanorods on tumor cells," *Nanomedicine*, Vol. 2, No. 1, Pp. 125-32 (2007).

20. X. Huang, P.K. Jain, I.H. El-Sayed and M.A. El-Sayed, "Determination of the Minimum Temperature Required for Selective Photothermal Destruction of Cancer Cells with the Use of Immunotargeted Gold Nanoparticles," *Photochemistry and Photobiology*, Vol. 82, No. 2, Pp. 412-7 (2006).

21. D. Kim, S. Park, J.H. Lee, Y.Y. Jeong and S. Jon, "Antibiofouling Polymer-Coated Gold Nanoparticles as a Contrast Agent for in Vivo X-ray Computed Tomography Imaging," *Journal of the American Chemical Society*, Vol. 129, No. 24, Pp.7661-5 (2007).

22. J.F. Hainfeld, D.N. Slatkin and H.M. Smilowitz, "The use of gold nanoparticles to enhance radiotherapy in mice," *Physics in Medicine and Biology*, Vol. 49, N309 (2004).

23. B.D. Chithrani, A.A. Ghazani and W.C.W.Chan, "Determining the Size and Shape Dependence of Gold Nanoparticle Uptake into Mammalian Cells," *Nano Letters*, Vol. 6, No. 4, Pp. 662-8 (2006).

24. B.D. Chithrani and W.C.W. Chan, "Elucidating the Mechanism of Cellular Uptake and Removal of Protein-Coated Gold Nanoparticles of Different Sizes and Shapes," *Nano Letters*, Vol. 7, No. 6, Pp. 1542-50 (2007).

25. J.M. de la Fuente and C.C. Berry, "Tat Peptide as an Efficient Molecule To Translocate Gold Nanoparticles into the Cell Nucleus," *Bioconjugate Chemistry*, Vol. 16, No. 5, Pp. 1176-80 (2005).

26. M. Lewin, N. Carlesso, C.H. Tung, X.W. Tang, D. Corry, D.T. Scadden and R. Weissleder, "Tat peptide-derivatized magnetic nanoparticles allow in vivo tracking and recovery of progenitor cells," *Nature Biotechnology, Vol.* 18, Pp. 410–414 (2000).

27. A.K. Salem, P.C. Searson and K.W. Leong, "Multifunctional nanorods for gene delivery," *Nature Materials*, Vol. 2, Pp. 668–671 (2003).

28. S.D. Brown, P. Nativo, J-A. Smith, D. Stirling, P.R. Edwards, B. Venugopal, D.J. Flint, J.A. Plumb, D. Graham and N.J. Wheate, "Gold Nanoparticles for the Improved Anticancer Drug Delivery of the Active Component of Oxaliplatin," *Journal of the American Chemical Society*, Vol. 132, No. 13, Pp. 4678-84 (2010).

29. K. Raj, B. Moskowitz and R. Casciari, "Advances in ferrofluid technology," *Journal of Magnetism and Magnetic Materials*, Vol. 149, No. 1-2, Pp. 174-80 (1995).

30. D. Speliotis, "Magnetic recording beyond the first 100 Years," *Journal of Magnetism and Magnetic Materials*, Vol. 193, No. 1-3, Pp. 29-35 (1999).

31. R. Qiao, C. Yang and M. Gao, "Superparamagnetic iron oxide nanoparticles: from preparations to in vivo MRI applications," *Journal of Materials Chemistry*, Vol. 19, No. 35, Pp. 6274-93 (2009).

32. M. Mahmoudi, S. Sant, B. Wang, S. Laurent and T. Sen, "Superparamagnetic iron oxide nanoparticles (SPIONs): Development, surface modification and applications in chemotherapy," *Advanced Drug Delivery Reviews*, Vol. 63, No. 1-2, Pp. 24-46 (2011).

33. A.K. Gupta and M. Gupta, "Synthesis and surface engineering of iron oxide nanoparticles for biomedical applications," *Biomaterials*, Vol. 26, No. 18, Pp. 3995-4021 (2005).

34. P. Xu, G.M. Zeng, D.L. Huang, C.L. Feng, S. Hu, M.H. Zhao, C. lai, Z. Wei, C. Huang, G.X. Xie and Z. H. Liu, "Use of iron oxide nanomaterials in wastewater treatment: A review," *Science of Total Environment*, Vol. 424, Pp. 1-10 (2012).

35. G.F. Goya, T.S. Berquó, F.C. Fonseca and M.P. Morales, "Static and dynamic magnetic properties of spherical magnetite nanoparticles," *Journal of Applied Physics*, Vol. 94, Pp. 3520-8 (2003).

36. C.P. Bean, "Hysteresis Loops of Mixtures of Ferromagnetic Micropowders," *Journal of Applied Physics*, Vol. 26, Pp. 1381-3 (1955).

37. J. Frenkel and J. Dorfman, "Spontaneous and Induced Magnetisation in Ferromagnetic Bodies," *Nature*, Vol. 126, Pp. 274-5 (1930).

38. C. Kittel, "Theory of the Dispersion of Magnetic Permeability in Ferromagnetic Materials at Microwave Frequencies," *Physical Review*, Vol. 70, No. 5-6, Pp. 281-90 (1946).

39. C.P. Bean and J.D. Livingston, "Superparamagnetism," *Journal of Applied Physics*, Vol. 30, Pp. S120-S9 (1959).

40. G.A. Candela and R.A. Haines, "A method for determining the region of superparamagnetism," *Applied Physics Letters*, Vol. 34, Pp. 868-70 (1979).

41. E. J. W. Verwey, "Electronic conduction of magnetite and its transition point at low temperatures," *Nature*, Vol. 144, Pp. 327-8 (1939).

42. J. Wang, Q. Chen, X. Li, L. Shi, Z. Peng and C. Zeng, "Disappearing of the Verwey transition in magnetite nanoparticles synthesized under a magnetic field: implications for the origin of charge ordering," *Chemical Physics Letters*, Vol. 390, No. 1-3, Pp. 55-8 (2004).

43. Y. Sahoo, A. Goodarzi, M.T. Swihart, T.Y. Ohulchanskyy, N Kaur, E.P. Furlani and P.N. Prasad, "Aqueous Ferrofluid of Magnetite Nanoparticles: Fluorescence Labeling and Magnetophoretic Control," *The Journal of Physical Chemistry B*, Vol. 109, No. 9, Pp. 3879-85 (2005).

44. P.S. Stephen, *Low viscosity magnetic fluid obtained by the colloidal suspension of magnetic particles*, US Patent 3215572 (1965).

45. Y-G. Zhao, H-Y Shen, S-D Pan and M-Q. Hu, "Synthesis, characterization and properties of ethylenediamine-functionalized Fe3O4 magnetic polymers for removal of Cr(VI) in wastewater," *Journal of Hazardous Materials*, Vol. 182, No. 1-3, Pp. 295-302 (2010).

46. S.R. Chowdhury and E.K. Yanful, "Arsenic and chromium removal by mixed magnetite–maghemite nanoparticles and the effect of phosphate on removal," *Journal of Environmental Management*, Vol. 91, No. 11, Pp. 2238-47 (2010).

47. J. Hu, G. Chen and I.M.C. Lo, "Removal and recovery of Cr(VI) from wastewater by maghemite nanoparticles," *Water Research*, Vol. 39, No. 18, Pp. 4528-36 (2005).

48. K. J. Widder, A.E. Senyei and D.F. Ranney, "In vitro release of biologically active adriamycin by magnetically responsive albumin microspheres," *Cancer Research*, Vol. 40, Pp. 3512–7 (1980).

49. J. M. Gallo, C.T. Hung, P.K. Gupta and P.G. Perrier, "Physiological pharmacokinetic model of adriamycin delivered via magnetic albumin microspheres in the rat," *Journal of Pharmacokinetics and Biopharmaceutics*, Vol. 17, No. 3, Pp. 305–26 (1989).

50. S. Laurent, D. Forge, M. Port, A. Roch, C. Robic, L. Vander Elst and R. N. Muller, "Magnetic Iron Oxide Nanoparticles: Synthesis, Stabilization, Vectorization, Physicochemical Characterizations, and Biological Applications," *Chemical Reviews*, Vol. 108, No. 6, Pp. 2064-110 (2008).

51. A-H Lu, E.L. Salabas and F. Schüth, "Magnetic Nanoparticles: Synthesis, Protection, Functionalization, and Application," *Angewandte Chemie International Edition*, Vol. 46, No. 8, Pp. 1222-44 (2007).

52. J-P Jolivet, C. Chaneac and E. Tronc, "Iron oxide chemistry. From molecular clusters to extended solid networks," *Chemical Communications*, No. 5, Pp. 481-3 (2004).

53. N.M. Gribanov, E.E. Bibik, O.V. Buzunov and V.N. Naumov, "Physico-chemical regularities of obtaining highly dispersed magnetite by the method of chemical condensation," *Journal of Magnetism and Magnetic Materials*, Vol. 85, No. 1-3, Pp. 7-10 (1990).

54. W.C. Elmore, "Ferromagnetic Colloid for Studying Magnetic Structures," *Physical Review Letters*, Vol. 54, Pp. 309-10 (1938).

55. T.J. Daou, G. Pourroy, S. Bégin-Colin, J.M. Grenèche, C. Ulhaq-Bouillet, P. Legaré, P. Bernhardt, C. Leuvrey and G. Rogez, "Hydrothermal Synthesis of Monodisperse Magnetite Nanoparticles," *Chemistry of Materials*, Vol. 18, No. 18, Pp. 4399-404 (2006).

56. S. Sun S and H. Zeng, "Size-Controlled Synthesis of Magnetite Nanoparticles," *Journal of the American Chemical Society*, Vol. 124, No. 28, Pp. 8204-5 (2002).

57. Z. Xu, C. Shen, Y. Hou, H. Gao and S. Sun, "Oleylamine as Both Reducing Agent and Stabilizer in a Facile Synthesis of Magnetite Nanoparticles," *Chemistry of Materials*, Vol. 21, No. 9, Pp. 1778-80 (2009).

58. H. Zeng and S. Sun, "Syntheses, Properties, and Potential Applications of Multicomponent Magnetic Nanoparticles," *Advanced Functional Materials*, Vol. 18, No. 3, Pp. 391-400 (2008).

59. N. Lewinski, V. Colvin and R. Drezek, "Cytotoxicity of Nanoparticles," *Small*, Vol. 4, No. 1, Pp. 26-49 (2008).

60. G.A. Sotiriou, "Biomedical applications of multifunctional plasmonic nanoparticles," *Wiley Interdisciplinary Reviews: Nanomedicine Nanobiotechnology*, Vol. 5, No. 1, Pp. 19-30 (2013).

VITA

Akshay Pariti was born on January 17, 1991 in Bangalore, India and brought up in Hyderabad, India. He obtained his undergraduate degree in Biotechnology from Manipal Institute of Technology (MIT), Manipal, India in 2012. During his senior year, he worked on the project titled "Treatment of Dairy Wastewater by Trickling Filter", under the supervision of Dr. Ramananda Bhat. His work involved designing, fabrication and evaluation of the trickling filter by chemical analysis of the influent and effluent wastewater. After his graduation, in Fall 2012 he started graduate studies in Chemical Engineering at Missouri University of Science and Technology, Rolla, Missouri.

During his course of study, he has worked on synthesis, characterization and functionalization of superparamagnetic gold-iron oxide nanoparticles for medicinal applications (specifically, for hyperthermia). He received his M.S. degree in Chemical Engineering from Missouri University of Science and Technology in August, 2014.